BIOMECHANICAL RESPONSE OF THE HUMAN EYE TO DYNAMIC IMPACT

Jill Aliza Bisplinghoff

Thesis submitted to the faculty of the
Virginia Polytechnic Institute and State University
in partial fulfillment of the requirements for the degree of

Master of Science

In

Biomedical Engineering

Stefan M. Duma, PhD, Chair

H. Clay Gabler, PhD

Warren N. Hardy, PhD

Joel D. Stitzel, PhD

April 10, 2009

Blacksburg, Virginia

Keywords: eye, injury, risk, material properties, stress, strain, rupture, sclera, pressure,

Copyright 2009, Jill A. Bisplinghoff

BIOMECHANICAL RESPONSE OF THE HUMAN EYE TO DYNAMIC IMPACT

Jill Aliza Bisplinghoff

ABSTRACT

Blindness due to ocular trauma is a significant problem in the United States considering that each year approximately 500,000 years of eyesight are lost. The most likely sources of eye injuries include sports related impacts, automobile accidents, consumer products, and military combat. Out of the 1.9 million total eye injuries in the country, more than 600,000 sports injuries occur each year and 40,000 of them require emergency care. In 2007, approximately 66,000 people suffered from vehicle related eye injuries in the United States. Of the vehicle occupants sustaining an eye injury during a crash, as many as 15% to 25% sustained severe eye injuries and it was shown that within these severe eye injuries as many as 45% resulted in globe rupture.

The purpose of this thesis is to characterize the biomechanical response of the human eye to dynamic loading. A number of test series were conducted with different loading conditions to gather data. A drop tower pressurization system was used to dynamically increase intraocular pressure until rupture. Results for rupture pressure, stress and strain were reported. Water streams that varied in diameter and velocity were developed using a customized pressure system to impact eyes. Intraocular pressure, normalized energy and eye injury risk were reported. A Facial and Ocular Countermeasure Safety (FOCUS) headform was used to measure the force applied to a synthetic eye during each hit from projectile shooting toys. The risk of eye injury for each impact was reported. These data provide new and significant research to the field of eye injury biomechanics to further the understanding of eye injury thresholds.

ATTRIBUTION

Several colleagues and coworkers aided in the research behind several of the chapters of this thesis. A brief description of their background and their contributions are included here.

Stefan Duma- Ph.D. (Department of Mechanical Engineering, Virginia Tech) is the primary Advisor and Committee Chair. Dr. Duma provided guidance, counsel and the needed funding for the work in this thesis.

Chapter 1: High Rate Internal Pressurization of Human Eyes to Predict Globe Rupture

Craig McNally (Research Engineer, Virginia Tech) currently at Virginia Tech working as a research engineer in the Center for Injury Biomechanics. Craig was involved in the design and construction of the test setup for this Chapter 1.

Chapter 2: Dynamic Material Properties of the Human Sclera

Craig McNally (Research Engineer, Virginia Tech) currently at Virginia Tech working as a research engineer in the Center for Injury Biomechanics. Craig was involved in the design and construction of the test setup for this Chapter 2.

Sarah Manoogian- Ph.D. (Department of Mechanical, Virginia Tech) is employed by Biodynamic Research Corporation and worked in collaboration with the author on a project. Sarah contributed to the discussion of calculating stress and strain of the human sclera in Chapter 2.

Chapter 5: Evaluation of Eye Injury Risk from Projectile Shooting Toys using the FOCUS Headform

TABLE OF CONTENTS

Abstract ii

Table of Contents iii

List of Figures vi

List of Tables viii

Chapter 1: High Rate Internal Pressurization of Human Eyes to Predict Globe Rupture 1

- Abstract 1
- Introduction 1
- Methods 3
- Results 5
- Comment 7
- Acknowledgements 10
- References 10

Chapter 2: Dynamic Material Properties of the Human Sclera 12

- Abstract 12
- Introduction 12
- Materials and Methods 13
- Results 17
- Discussion 20
- Acknowledgements 23
- References 23

Chapter 3: Intraocular Pressure during High Speed Projectile Impacts 25

- Abstract 25
- Introduction 25
- Methods 26
- Results 28
- Comment 31
- Acknowledgements 34
- References 34

Chapter 4: Eye Injury Risk from Water Stream Impact 36
Abstract 36
Introduction 36
Methods 38
Results 40
Comment 44
Acknowledgements 46
References 46
Chapter 5: Evaluation of Eye Injury Risk from Projectile Shooting Toys using the FOCUS Headform 48
Abstract 48
Introduction 48
Methodology 49
Results 52
Discussion 54
Conclusion 55
Acknowledgements 56
References 56
Chapter 6: Summary of research 57

LIST OF FIGURES

Figure 1: Globe rupture: (Left) A baseball impact with a human eye within a gelatin orbit (pre-impact). (Center) A baseball impact with a human eye within a gelatin orbit resulting in rupture. (Right) Globe rupture in a human eye. 2

Figure 2: Schematic of pressure system used to examine high rate rupture pressures of human eyes. 4

Figure 3: Rupture pressure with respect to time for 20 human eyes. 7

Figure 4: Pressure difference between upstream pressure and direct internal eye pressure. 8

Figure 5: Schematic of high rate pressurization system (left) used to determine material properties and the expansion of a human eye shown with optical markers (right)... 14

Figure 6: Progression of the expansion of the markers until rupture for test # 11. 18

Figure 7: Stress-strain curve responses in the equatorial direction of 12 eye rupture tests. 18

Figure 8: Stress-strain curve response in the meridional direction of 12 eye rupture tests. 19

Figure 9: Comparison of previous stress-strain curves to current study. 20

Figure 10: Stress and strain comparison for test with rupture close to and away from optical markers in the meridional direction. 21

Figure 11: Experimental testing was performed used a pneumatically powered cannon in an enclosed shooting volume to impact porcine eyes. 27

Figure 12: Relative size differences of the three projectiles compared to a penny (Left to Right: penny, large aluminum rod, small aluminum rod, small metal ball). 28

Figure 13: High speed video documentation of a test with the 6.35 mm metal ball projectile. 29

Figure 14: Correlation between internal eye pressure and kinetic energy. 32

Figure 15: Correlation between internal eye pressure and normalized energy at full range with the human rupture pressure threshold at 11894 mmHg and the porcine rupture pressure threshold at 16342 mmHg. 33

Figure 16: Water stream system used to impact porcine eyes. 38

Figure 17: Intraocular pressure response for the three nozzle sizes at a water velocity of 3 m/s. 41

Figure 18: High speed video of a test with a 9.525 mm water stream at 4.23 m/s. 41

Figure 19: Influence of nozzle diameter and velocity based on intraocular pressure..... 45

Figure 20: (Left) Experimental setup with the FOCUS headform and the ball launcher. (Right) Relative size comparison of the three projectiles. Top to bottom: ball, foam launcher, dart. 50

Figure 21: Injury risk curves for corneal abrasion, hyphema, lens dislocation, retinal damage, and globe rupture as a function of normalized energy from published research. 52

LIST OF TABLES

Table 1: Rupture pressure results for 20 human eyes. 6

Table 2: True stress and True strain results for 12 human eyes..... 19

Table 3: Internal eye pressure, normalized energy and velocity results for the small aluminum rod projectile. (mass = 3.61 g, diameter = 9.25 mm)..... 29

Table 4: Internal eye pressure, normalized energy and velocity results for the large aluminum rod projectile. (mass = 5.19 g, diameter = 11.16 mm)..... 30

Table 5: Internal eye pressure, normalized energy and velocity results for the small metal ball projectile. (mass = 1.02 g, diameter = 6.35 mm) 30

Table 6: Injury risk function coefficients from published research. 40

Table 7: Internal eye pressure, velocity and injury risk results for the 3.175 mm nozzle diameter water stream. 42

Table 8: Internal eye pressure, velocity and injury risk results for the 6.35 mm nozzle diameter water stream. 43

Table 9: Internal eye pressure, velocity and injury risk results for the 9.525mm nozzle diameter water stream. 44

Table 10: Injury risk function coefficients from published research. 51

Table 11: Globe rupture injury risk results from FOCUS eye load cell injury risk criteria. 53

Table 12: Injury risk results using the normalized energy method for corneal abrasion, hyphema, lens dislocation, retinal damage, and globe rupture. 54

Table 13: List of publications as an outcome of this thesis. 57

CHAPTER 1: HIGH RATE INTERNAL PRESSURIZATION OF HUMAN EYES TO PREDICT GLOBE RUPTURE

ABSTRACT

Objectives: To determine the dynamic rupture pressure of the human eye using an in vitro high rate pressurization system to investigate blunt impact eye injuries.

Methods: Internal pressure was dynamically induced into the eye using a drop tower pressurization system. The internal eye pressure was measured with a small pressure sensor inserted into the eye through the optic nerve. A total of 20 human eye tests were performed to determine rupture pressure and characterize rupture patterns.

Results: The high rate pressurization resulted in a mean rupture pressure of 0.97 ± 0.29 MPa (7275.60 ± 2175.18 mm Hg). A total of 16 ruptured in the equatorial direction while 4 ruptured in the meridional direction. There is not a significant difference in the rupture pressure between the equatorial and meridional directions (p=0.16).

Conclusions: As the loading rate increases, the rupture pressure of the human eye increases.

Clinical Relevance: Eye injuries are expensive to treat given the estimated annual cost associated with adult vision problems in the United States is $51.4 billion. Determining globe rupture properties will establish injury criteria for the human eye to prevent these common yet devastating injuries.

INTRODUCTION

Over 1.9 million people suffer from eye injuries in the United States each year [1]. Automobile accidents[2-7], sports related impacts[8, 9], consumer products, and military combat[10] are some of the causes of the severe eye injuries endured [11]. These injuries are expensive to treat given the estimated annual cost associated with adult vision problems in the United States is $51.4 billion[12, 13]. Out of the total number of eye injuries in the country, more than 600,000 sports injuries occur each year and 40,000 of them require emergency care[14]. In a 2002 study it was found that over 9000 globe ruptures occur in the United States each year[15]. A blunt impact, like that of a baseball, will cause the eye

to compress with an increase in internal pressure which can result in globe rupture (Figure 1). The rupture initiates away from the impact location, demonstrating that the rupture occurs from the increase in internal pressure. Determining globe rupture properties will provide the needed information for establishing injury criteria for the human eye to help prevent these common yet devastating injuries.

Figure 1: Globe rupture: (Left) A baseball impact with a human eye within a gelatin orbit (pre-impact). (Center) A baseball impact with a human eye within a gelatin orbit resulting in rupture. (Right) Globe rupture in a human eye.

Safe intraocular pressures are of particular use to the clinical ophthalmologist[16]. In published research, the rupture pressure of eyes has been examined to determine the effect of ocular surgery[5, 16-20], and only one study has been published on the rupture pressure of healthy human eyes [21]. Burnstein et al.[17] studied the strength of postmortem human and porcine eyes after undergoing photorefractive keratectomy by increasing intraocular pressure (IOP) gradually with nitrogen gas until globe rupture occurred. The eye was attached to the nitrogen gas system by a 25-gauge butterfly needle that was inserted into the anterior chamber at the limbus. Pressure was increased by 0.03 MPa (225.02 mm Hg) at 5-second intervals. Burnstein found the rupture pressure of human eyes subjected to photorefractive keratectomy to be 0.46 ± 0.12 MPa (3450.28 ± 900.07 mm Hg), while porcine eyes subjected to photorefractive keratectomy were observed to rupture at 0.53 ± 0.10 MPa (3975.33 ± 750.06 mm Hg). In 2 eyes undergoing phototherapeutic keratectomy, Burnstein et al. found rupture pressures of 0.55 MPa (4125.34 mm Hg) and 0.68 MPa (5100.42 mm Hg). Voorhies performed both static and dynamic tests on healthy postmortem human and porcine eyes with similar methodology[21]. The static rupture pressure for human eyes was found to be 0.36 ± 0.20

MPa (2700.22 ± 1500.12 mm Hg); whereas the dynamic rupture pressure was found to be 0.91 ± 0.29 MPa (6825.56 ± 2175.18 mm Hg).

The previous studies have tested human and porcine eyes to rupture; however, these studies are limited in that no high rate dynamic tests were performed that would realistically simulate a dynamic ocular injury, such as sports related injuries, automobile injuries, military combat, or injuries caused by consumer products [17, 21, 22]. Moreover, the majority of these studies were focused on testing specimens subjected to corrective eye surgery prior to testing with segmented eye tissue. Therefore the purpose of this study is to analyze the high rate rupture pressure of healthy human eyes using an internal pressurization system.

METHODS

High rate pressurization was accomplished with a custom pressure system that was built to examine rupture properties of the human eye (Figure 2). The test setup consisted of a drop tower that was used to create a hydraulic system to pressurize the human eye in a dynamic event. To initiate the event a weight was dropped onto a piston which was inserted into the hydraulic cylinder. Preparation of the system included adding water through the cylinder to act as the medium for pressurization and to produce an approximate initial intraocular pressure of 0.002 MPa (15.00 mm Hg) before rupture. Connecting the eye to the system was a 16-gage intravenous needle inserted into the optic nerve (Figure 2). In order to secure the optic nerve to the needle a medical suture was used while a cylindrical placement guide held the eye in place below the needle. To ensure that the optic nerve was sealed it was covered with a flexible coupling and then secured with a plastic fastener.

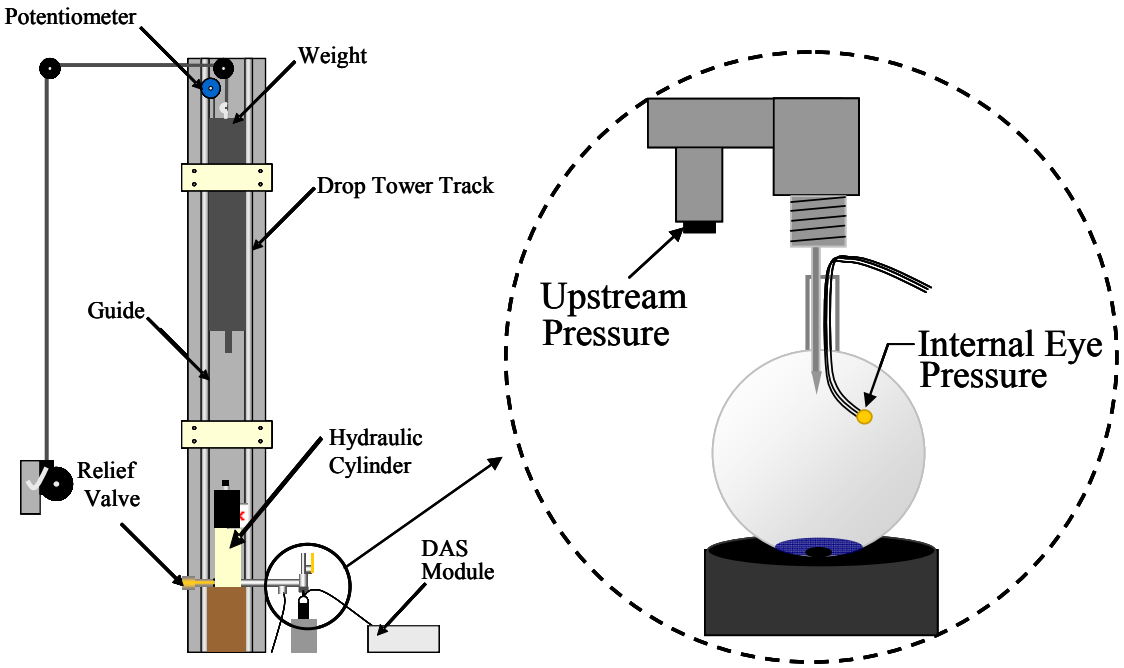

Figure 2: Schematic of pressure system used to examine high rate rupture pressures of human eyes.

The high rate dynamic event occurred when the weight was suspended above the piston at a height of 17.78 cm and then released. The impact of the weight onto the piston caused the water to be displaced throughout the system, which created a high rate increase in intraocular pressure resulting in the rupture of the eye. In order to capture this event, high speed video and data acquisition were used. A Photron Ultima APX-RS camera (Photron Inc, San Diego, CA) captured video at 10,000 frames per second with a resolution of 512x512, while the data acquisition system (DAS) collected data at 30,000 Hz. The pressure transducer data and the high-speed video were correlated to determine the pressure at the time of rupture.

In order to acquire the internal pressure of the human eye, an in situ pressure sensor was utilized. A small pressure sensor (Precision Measurement Company, Model 060, Ann Arbor, MI) was inserted into the eye through the optic nerve. The pressure transducer was rated for a range of 0-3.45 MPa (0-25877.13 mm Hg) and a frequency response of 10,000 Hz which are ideal for this application.

Twenty human eyes were procured from the Roanoke Eye Bank (Roanoke, VA) and the North Carolina Eye Bank (Winston-Salem, NC). No corneal transplantation or other operations were done to the eyes prior to testing. The eyes were never frozen and kept in a saline solution in glass jars and refrigerated until testing. A previous study showed the lack of correlation between age and rupture pressure, as well as, time from harvest to test and rupture pressure [4]. Statistical analyses were performed using a student T-test with α=0.05 used to determine statistical significance. All test procedures were reviewed and approved by the Virginia Tech Institutional Review Board.

RESULTS

The high rate pressurization of 20 human eyes resulted in a mean rupture pressure of 0.97 ± 0.29 MPa (7275.60 ± 2175.18 mm Hg) (Table 1). The failure pressure ranged from 0.57 MPa (4275.35 mm Hg) to 1.59 MPa (11925.98 mm Hg) (Figure 3). The dynamic loading rate was 36.50 ± 15.35 MPa/s (273772.5 ± 115134.5 mm Hg/s) for the 20 human eye tests. High speed video for each test showed the location of each rupture. Out of the 20 eyes tested, 18 ruptured at the equator, while the remaining 2 ruptured through the cornea. The eyes were then examined to determine the direction of the rupture. From inspection it was found that 4 ruptured in the meridional direction while 16 ruptured in the equatorial direction. A student T-test revealed that the difference in the rupture pressure between the equatorial mean of 0.93 ± 0.30 MPa (6975.57 ± 2250.19 mm Hg) and the meridional mean of 1.13 ± 0.21 MPa (8475.70 ± 1575.13 mm Hg) was not significant (p=0.16).

Table 1: Rupture pressure results for 20 human eyes.

Test Number	Cadaver Number	Rupture Pressure, MPa	Time to Rupture, ms	Loading Rate, MPa/s	Rupture Direction	Rupture Location
1	1775-07-02	1.59	20.6	77.4	equatorial	equator
2	1771-07-01	0.70	21.2	32.8	equatorial	equator
3	1771-07-02	0.82	21.5	38.3	equatorial	equator
4	1775-07-01	0.80	23.8	33.7	equatorial	equator
5	1733-07-01	1.34	24.5	54.7	equatorial	equator
6	1731-07-02	1.30	25.2	51.6	meridional	equator
7	1731-07-01	1.32	25.2	52.4	meridional	equator
8	1733-07-02	1.50	25.6	58.6	equatorial	equator
9	1777-07-01	0.71	26.1	27.1	equatorial	equator
10	1747-07-02	0.57	26.5	21.6	equatorial	cornea
11	1739-07-02	0.95	26.8	35.3	meridional	cornea
12	1747-07-01	0.78	28.1	27.7	equatorial	equator
13	1739-07-01	0.91	28.7	31.7	equatorial	equator
14	1772-07-01	0.96	28.8	33.5	meridional	equator
15	1791-07-01	1.01	29.3	34.4	equatorial	equator
16	1791-07-02	0.98	29.8	32.9	equatorial	equator
17	0708-0209-1	0.94	31.5	30.0	equatorial	equator
18	0708-0209-2	0.88	37.3	23.7	equatorial	equator
19	0708-0136-1	0.76	39.0	19.5	equatorial	equator
20	0708-0136-2	0.60	45.9	13.2	equatorial	equator
Average		0.97	28.3	36.5		
Standard deviation		0.29	6.2	15.3		

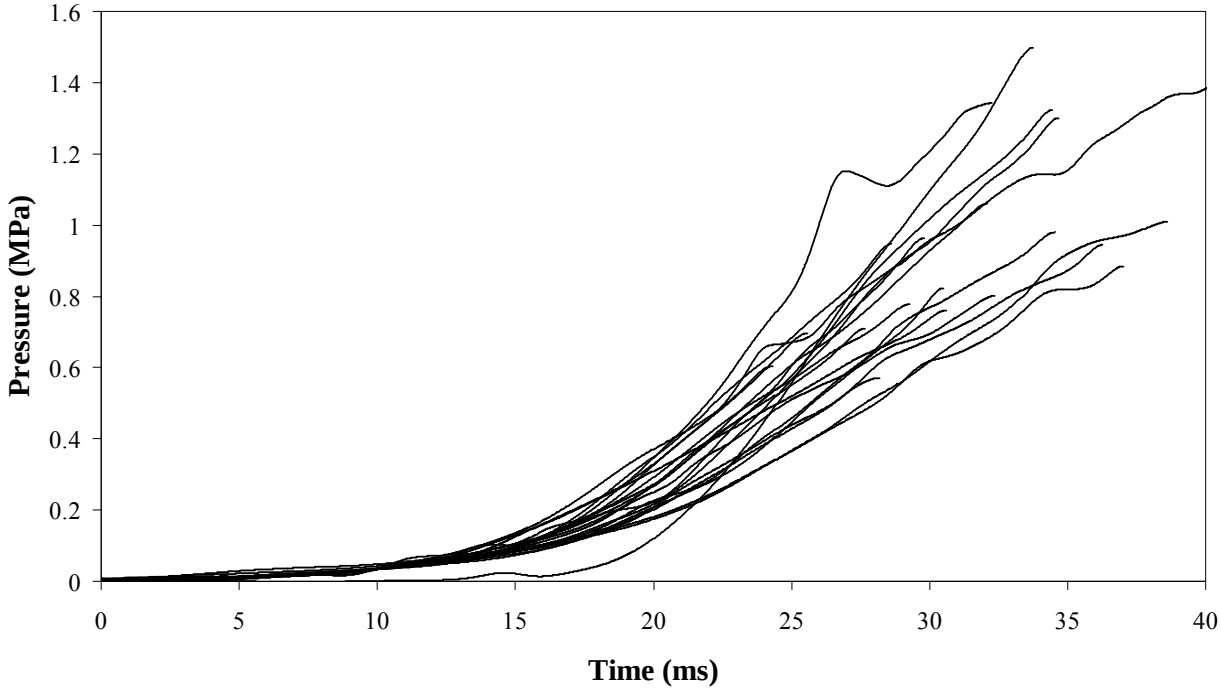

Figure 3: Rupture pressure with respect to time for 20 human eyes.

COMMENT

Previous studies have performed quasi-static and dynamic tests to determine the rupture pressure of human eyes[17, 18, 21-23]. Both Campos and Pinheiro tested the effects of refractive surgery. Campos used porcine eyes and was unable to report rupture pressure results due to the capability of the manometer used [18]. The test series completed by Pinheiro utilized an artificial anterior chamber to investigate the integrity of the cornea; therefore determining rupture pressure for the cornea rather than the sclera[22]. Although these studies are useful for their specific purpose, the current study is intended as a more general approach that can be applied for applications concerning scleral injuries that occur from increasing internal pressure, such as a blunt impact.

From Burnstein, Uchio, and Voorhies it has been observed that the human eye is both anisotropic and viscoelastic[17, 21, 23]. Previous dynamic tests performed by Voorhies were executed using a loading rate of approximately 2.77 MPa/s (20776.71 mm Hg)[21]; however for the current test series a higher loading rate was desired to more accurately

predict a dynamic ocular injury observed from blunt object impacts. The high rate rupture pressure device achieved an average loading rate of 36.5 MPa/s (273772.5 mm Hg/s), which is an order of magnitude larger than the previous dynamic tests. In this study both the loading rate and the duration of the event were changed by approximately an order of magnitude from previous dynamic tests [21]. The time to rupture was also measured and resulted in a mean of 28.27 ± 6.26 ms, compared to 0.46 ± 0.23 seconds from previous dynamic tests performed by Voorhies[21].

In the previous study by Voorhies[21], a pressure transducer was placed at a location before the needle interface between the eye and the system and was assumed to reflect the internal pressure of the human eye[21]. In comparing the current results with the previous rupture pressure data, it is important to note that due to pressure loss across the needle during the event the upstream pressure used for the previous testing presents a higher pressure than is actually experienced by the eye (Figure 4). There is a measurement error that is introduced when the upstream pressure is used instead of the direct internal pressure.

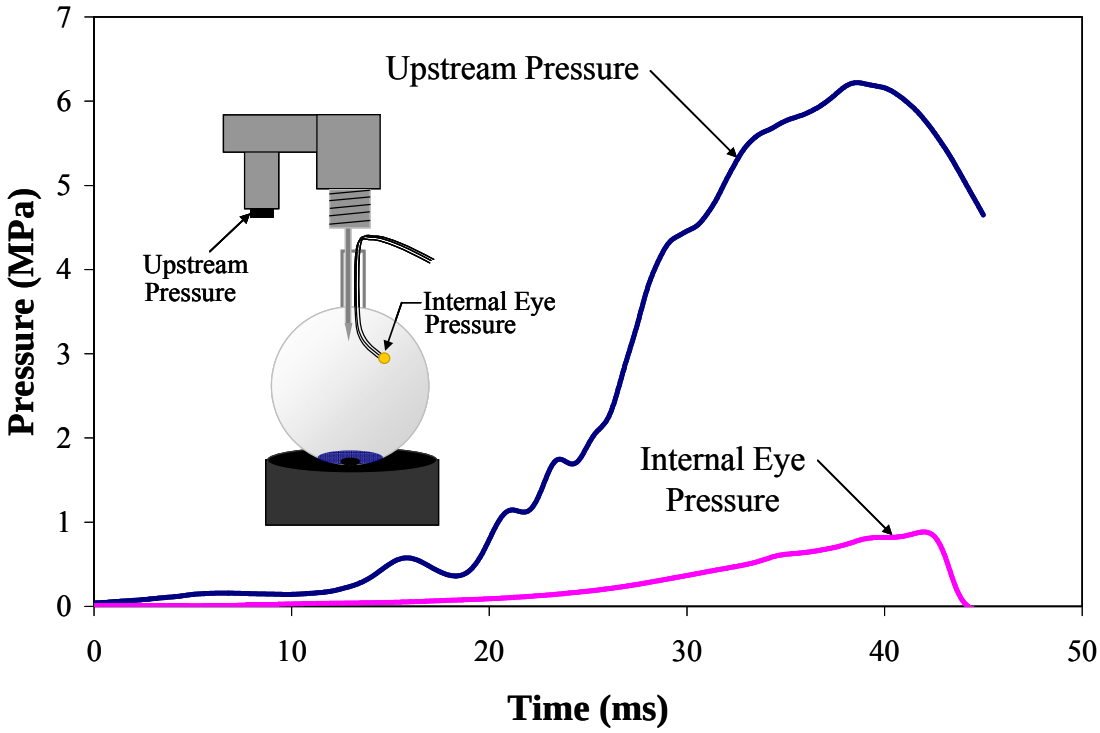

Figure 4: Pressure difference between upstream pressure and direct internal eye pressure.

The location of the pressure sensor inside the eye was also a concern due to the change in pressure gradient as the water was injected into the eye. A test was done with two sensors within one eye to compare the results of two identical pressure sensors in different locations during the event. The response shows that regardless of the location of the pressure sensors the pressure output is the same.

All eyes were stored in saline and were refrigerated prior to testing. It has been noted that sclera is largely acellular and its strength comes from collagen fibers similar to those found in ligaments [4]. Since the tissue was never exposed to a freeze-thaw cycle and was stored in refrigerated saline, the globe's integrity was preserved before the testing. An analysis was done to show the lack of correlation between the rupture pressure and the time from the harvest to the test date which resulted in an R^2 value of 0.06.

The principal rupture location for the 20 tests was the equator. Other research has also shown the equator as the prime location for a rupture occurring from a blunt impact, such as a baseball[21, 24]. Because failures occur primarily at the equator of the eye, this study, along with previous studies[4], suggest that the equator is the weakest portion of the eye.

Accurate response characteristics of the eye must be known in order for a model to behave realistically and to predict when failure of local tissues would occur. Although the rupture location was primarily the equator, the ruptures occurred in two different directions: along the equator and along the meridian. A student T-test was performed to determine if the difference in the rupture pressure between the equatorial and meridional direction was significant. A p-value of 0.16 shows the lack of significance in the difference in rupture pressure for the two directions.

These data are essential for the continuing improvement of eye injury prediction. It is this research that will provide the necessary information to advance the current mathematical and computer models. From this ongoing development of better eye injury risk assessment, society will experience the benefits through the reduction of eye injuries from blunt impacts.

ACKNOWLEDGEMENTS

The authors would like to acknowledge the United States Army Aeromedical Research Laboratory for their support of this program. The authors would also like to acknowledge the Virginia Tech - Wake Forest Center for Injury Biomechanics for funding the tissue testing.

REFERENCES

1. McGwin G, Xie A, Owsley C. Rate of eye injury in the united states. *Archives of Ophthalmology.* 2005;123:970-976.

2. Duma SM, Jernigan MV, Stitzel JD, et al. The effect of frontal air bags on eye injury patterns in automobile crashes. *Arch Ophthalmol.* Nov 2002;120(11):1517-1522.

3. Fukagawa K, Tsubota K, Kimura C, et al. Corneal endothelial cell loss induced by air bags. *Ophthalmology.* 1993;100(12).

4. Kennedy EA, Voorhies KD, Herring IP, Rath AL, Duma SM. Prediction of severe eye injuries in automobile accidents: static and dynamic rupture pressure of the eye. *Association for the Advancement of Automotive Medicine.* 2004;48:165-179.

5. Kisielewicz LT, Kodama N, Ohno S, Uchio E. Numerical prediction of airbag caused injuries on eyeballs after radial keratotomy. *SAE International Congress and Exposition*. Detroit, Michigan; 1998.

6. Duma SM, Crandall JR. Eye injuries from airbags with seamless module covers. *The Journal of Trauma.* 2000;48(4):786-789.

7. Duma SM, Kress TA, Porta DJ, et al. Airbag-induced eye injuries: A report of 25 cases. *The Journal of Trauma.* 1996;41(1):114-119.

8. Kennedy EA, Ng TP, McNally C, Stitzel JD, Duma SM. Risk functions for human and porcine eye rupture based on projectile characteristics of blunt objects. *Stapp Car Crash Journal.* 2006;50:651-671.

9. Vinger PF, Duma SM, Crandall J. Baseball hardness as a risk factor for eye injuries. *Arch Ophthalmol.* Mar 1999;117(3):354-358.

10. Heier JS, Enzenauer RW, Wintermeyer SF. Ocular injuries and diseases at a combat support hospital in support of Operations Desert Shield and Desert Storm. *Archives of Ophthalmology.* 1993;111:795-798.

11. Kennedy EA, Inzana JA, McNally C, et al. Development and validation of a synthetic eye and orbit for estimating the potential for globe rupture due to specific impact conditions. *Stapp Car Crash Journal.* October 2007 2007;51:381-400.

12. Frick KD, Gower EW, Kempen JH, Wolff JL. Economic impact of visual impairment and blindness in the United States. *Arch Ophthalmol.* Apr 2007;125(4):544-550.

13. Rein DB, Zhang P, Wirth KE, et al. The economic burden of major adult visual disorders in the United States. *Arch Ophthalmol.* Dec 2006;124(12):1754-1760.

14. Hecker S. More than half a million americans suffer eye injuries from sports-related accidents: Lack of proper eye protection can lead to painful injuries, vision loss and even blindness. *Vision News.* 2007.
15. Smith D, Wrenn K, Stack LB. The epidemiology and diagnosis of penetrating eye injuries. *Academic Emergency Medicine.* 2002;9(3):209-213.
16. Bryant MR, McDonnell PJ. Constitutive laws for biomechanical modeling of refractive surgery. *Journal of Biomechanical Engineering.* 1996;118:473-481.
17. Burnstein Y, Klapper D, Hersh PS. Experimental globe rupture after excimer laser photorefractive keratectomy. *Archives of Ophthalmology.* 1995;113:1056-1059.
18. Campos M, Lee M, McDonnell PJ. Ocular integrity after refractive surgery: effects of photorefractive keratectomy, phototherapeutic keratectomy, and radial keratotomy. *Ophthalmic Surgery.* 1992;23(9):598-602.
19. Hanna KD, Jouve FE, Waring GO, Ciarlet PG. Computer simulation of arcuate and radial incisions involving the corneoscleral limbus. *Eye.* 1989;3:227-239.
20. Wray WO, Best ED, Cheng LY. A mechanical model for radial keratotomy: toward a predictive capability. *Journal of Biomechanical Engineering.* 1994;116:56-61.
21. Voorhies KD. *Static and dynamic stress/strain properties for human and porcine eyes*. Blacksburg: Mechanical Engineering, Virginia Tech; 2003.
22. Pinheiro MN, Bryant MR, Tayyanipour R, Nassaralla BA, Wee WR, McDonnell PJ. Corneal integrity after refractive surgery: effects of radial keratotomy and mini-radial keratotomy. *Ophthalmology.* 1995;102(2):297-301.
23. Uchio E, Ohno S, Kudoh J, Aoki K, Kisieleqicz LT. Simulation model of an eyeball based on finite element analysis on a supercomputer. *British Journal of Ophthalmology.* 1999;83:1106-1111.
24. Stitzel JD, Duma SM, Cormier JM, Herring IP. A nonlinear finite element model of the eye with experimental validation for the prediction of globe rupture. *Stapp Car Crash Journal.* 2002;46.

CHAPTER 2: DYNAMIC MATERIAL PROPERTIES OF THE HUMAN SCLERA

ABSTRACT

As a result of trauma, approximately 30,000 people become blind in one eye every year in the United States. A common injury prediction tool is computational modeling, which requires accurate material properties to produce reliable results. Therefore, the purpose of this study was to determine the dynamic material properties of the human sclera. A high rate pressurization system was used to create dynamic pressure to the point of rupture in 12 human eyes. Measurements were obtained for the internal pressure, the diameter of the globe, the thickness of the sclera and the changing coordinates of the optical markers using high rate video. A relationship between true stress and true strain was determined for the sclera tissue in two directions. It was found that the average maximum true stress was 13.89 ± 4.81 MPa for both the equatorial and meridional directions, the average maximum true strain along the equator was 0.041 ± 0.014, and the average maximum true strain along the meridian was 0.058 ± 0.018. Results show a significant difference in the maximum strain in the equatorial and meridional directions ($p=0.02$). In comparing these data with previous studies, it is concluded that the human sclera is both anisotropic and viscoelastic. The dynamic material properties presented in this study can be used for advanced models of the human eye to help prevent eye injuries in the future.

INTRODUCTION

Over 1.9 million people suffer from eye injuries in the United States each year (McGwin, 2005). As a result of trauma, approximately 30,000 people become blind in one eye every year in the United States (Parver, 1986). In 2007, approximately 66,000 people suffered from vehicle related eye injuries in the United States (McGwin, 2005). Of the vehicle occupants sustaining an eye injury during a crash, as many as 15% to 25% sustain

severe eye injuries (Duma, 2000; Duma, 2002) and it was shown that within these severe eye injuries as many as 45% resulted in globe rupture (Kuhn, 1994).

Eye injuries have been a growing area of interest because of the increase in the frequency of these injuries in both the civilian and military sectors (Kennedy, 2007). In 1999 material properties for the sclera and cornea were developed using a uniaxial test setup to be incorporated in a finite element model (Uchio, 1999). Each globe was bisected at the equator and two strip samples of the sclera were taken from the corneoscleral limbus. Similar to a method used by Nash, Uchio measured the stress-strain relationship of the sclera by applying an axial force and measuring the change in length, cross sectional area and load (Nash, 1982; Uchio, 1999).

As a result of the sclera and cornea uniaxial material property study, several ocular computer models were created, most of which were focused on studying the effects of corrective eye surgery (Hanna, 1989; Sawusch, 1992; Wray, 1994; Bryant, 1996). The first dynamic computer model of the eye was created by Uchio and Kisielewicz (Kisielewicz, 1998; Uchio, 1999). This model found peak rupture stress using the uniaxial static material properties to be 9.4 MPa. A more recent and accurate model was created by Stitzel et al. called the Virginia Tech Eye Model (VTEM) (Stitzel, 2002). The VTEM was experimentally verified and developed to use a more realistic dynamic fluid-solid interaction modeling technique to simulate eye injuries. However, all previous studies were based on quasi-static properties (Battaglioli, 1984; Ahearne, 2007) and for more accurate rupture stress, dynamic material properties obtained without boundary condition limitations are more desirable. Therefore, the purpose of this study is to determine dynamic material properties for the human sclera.

MATERIALS AND METHODS

High rate intraocular pressurization was accomplished with a hydraulic system that consisted of a drop tower that was used to pressurize the human eye in a dynamic event (Figure 5). To initiate the event a weight was suspended above the piston at a desired

height of 17.78 cm and then released and dropped onto the piston which was inserted into the hydraulic cylinder. The impact of the weight onto the piston caused the water to be displaced throughout the system which created a high rate increase in intraocular pressure resulting in the rupture of the eye. This system created an average loading rate of 36.50 MPa/sec. This rate was selected to match internal pressure rates observed in baseball and automobile applications (Kennedy, 2006).

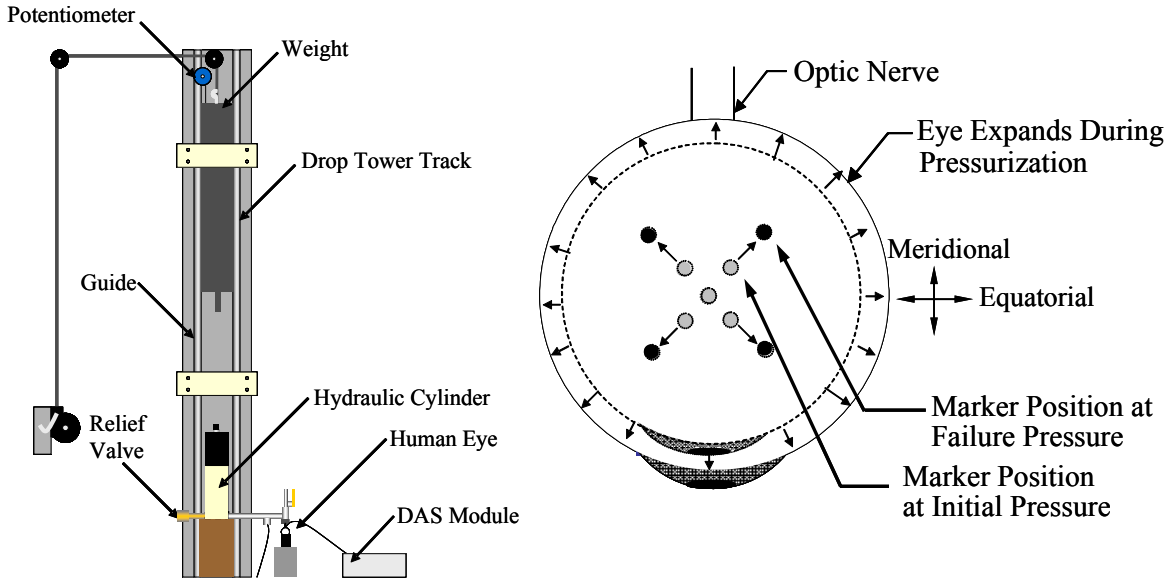

Figure 5: Schematic of high rate pressurization system (left) used to determine material properties and the expansion of a human eye shown with optical markers (right).

Preparation of the system included adding water through the cylinder to act as the medium for pressurization and to produce an initial intraocular pressure of 0.001993 MPa (8 inches of water). Connecting the eye to the system was a 16-gage intravenous needle inserted through the optic nerve. In order to secure the optic nerve to the needle a medical suture was used while a cylindrical placement guide held the eye in place below the needle. To ensure that the optic nerve was sealed it was covered with flexible coupling material and then secured with a plastic fastener.

Each human eye was stamped with 5 optical markers to provide a method for measuring strain (Figure 5). In order to capture this event, high speed video and data acquisition were used. A Photron Ultima APX-RS camera (Photron Inc, San Diego, CA) captured video at 10,000 frames per second with a resolution of 512x512, while the data

acquisition system (DAS) collected data at 30,000 Hz. The internal pressure of the eye was measured from a small pressure sensor inserted into the eye through the optic nerve. This was accomplished with a pressure transducer made by Precision Measurement Company (Model 060, Ann Arbor, MI). The pressure transducer was rated for a range of 0-3.45 MPa which was more than adequate for our expected pressure results and had a frequency response of 10 kHz.

Optical target tracking software was used to follow the movement of the diameter as well as the optical markers during the expansion of the eye (TEMA, Image Systems, Sweden). The accuracy of the tracking software was within 0.09 pixels and the video produced a pixel size at 12 pixels/mm. The internal pressure, optical marker tracking, and diameter data were correlated with respect to time.

The thickness of each specimen was examined with a high accuracy laser to determine the thickness of the sclera after testing. The specimens were sectioned at the location of the optical markers and kept in saline solution during the test procedure. Measurements were taken with a Microtrak II high speed laser with accuracy of 2.5 micrometers. This method reduced the effect of swelling that can occur with other histological processing methods.

Engineering stress (σ_E) was calculated using the internal pressure (P) with respect to time, along with the external radius (R) with respect to time (t) and the original thickness (T_1). Assuming that the eye is a spherical pressure vessel, the following equation was used to calculate the engineering stress in the eye:

$$\sigma_E = \frac{P(t) \cdot R(t)}{2T_1} \qquad (1)$$

The true stress σ_T was calculated using the same spherical pressure vessel equation but the change in thickness as the radius increased was added to the analysis (Eq.2). A relationship was derived to relate the radius and the thickness, where R_2 is the external

radius at time t, R_1 is the external radius at t=0, and r_1 is the internal radius at t=0 which is represented by Equation 3. Assuming that the sclera is incompressible and that there is no mass flowing into or out of the scleral shell, volume is constant throughout time. Through utilizing the equation for the volume of a shell, the thickness for each change in the radius was found (Eq.4) and used in Eq. 2 to find the true stress.

$$\sigma_T = \frac{P(t) \cdot R(t)}{2 \cdot T(r,t)} \tag{2}$$

$$r_1 = R_2 - T_1 \tag{3}$$

$$T = R_2 - \sqrt[3]{R_2^3 + r_1^3 - R_1^3} \tag{4}$$

Strain of the sclera was determined from the high speed video and the analysis software (TEMA) that was used to track the location of each of the 5 optical markers at each point in time. These data were then analyzed using a custom MATLAB code to calculate the True strain in both the equatorial and meridional directions. The deformation gradient tensor (F) for each group was determined by analyzing the position vectors (Eq.5), where x_i and y_i were the original positions of the markers and X_i and Y_i were the deformed positions of the markers. The True (Logarithmic) strain tensor (E) was found using Eq.6. A relationship between stress and strain was found for each of the twelve human eyes.

$$F = \left(\begin{bmatrix} X_1 & X_2 \\ Y_1 & Y_2 \end{bmatrix}_{t=n} \right) \left(\begin{bmatrix} x_1 & x_2 \\ y_1 & y_2 \end{bmatrix}_{t=0} \right)^{-1} \tag{5}$$

$$E = \begin{bmatrix} E_{11} & E_{12} \\ E_{21} & E_{22} \end{bmatrix} = \ln \sqrt{F \cdot F^T} \tag{6}$$

A characteristic average was calculated using a custom MATLAB code to clearly represent the stress-strain data (Lessley, 2004). This approach has been used in previous

studies and was used in the current study to better determine the average response and corridors to fit the data.

Twelve human eyes were acquired for testing, and no corneal transplantation or other operations were done to the eyes prior to procurement. The eyes were kept in a saline solution in glass jars and refrigerated for no longer than 15 days before they were tested. A previous study showed no correlation between donor age and rupture pressure, as well as, time from death and rupture pressure (Kennedy, 2004). A statistical analysis was performed using a matched pair student t-test to determine if a significance difference between the strain in the equatorial and meridional directions existed. All test procedures were reviewed and approved by the Virginia Tech Institutional Review Board.

RESULTS

As the intraocular pressure increased, the eye expanded until rupture occurred (Figure 6). The general trends of the stress-strain relationships for both directions are similar but show that there are significant directional effects present relative to strain ($p=0.02$) (Figure 7, Figure 8). The maximum strain for the equatorial direction ranged from 0.0193 to 0.0673 and the meridional direction ranges from 0.0262 to 0.0908. In comparison, the meridional direction showed significantly more strain than the equatorial direction ($p=0.02$). The true stress for the twelve tested eyes resulted in a range from 6.84 MPa to 20.37 MPa with an average of 13.89 ± 4.81 MPa (Table 2). Thickness was also measured and resulted in an average of 0.58 ± 0.13 mm. The characteristic average for both directions and the corresponding standard deviations show the directional effects (Figure 9).

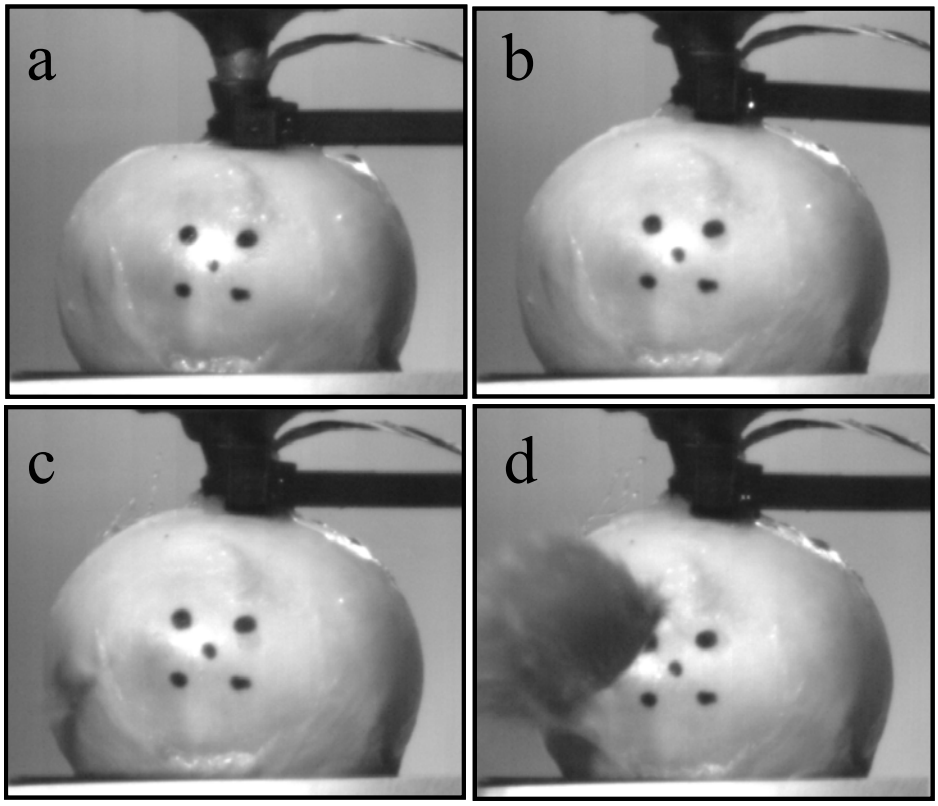

Figure 6: Progression of the expansion of the markers until rupture for test # 11.

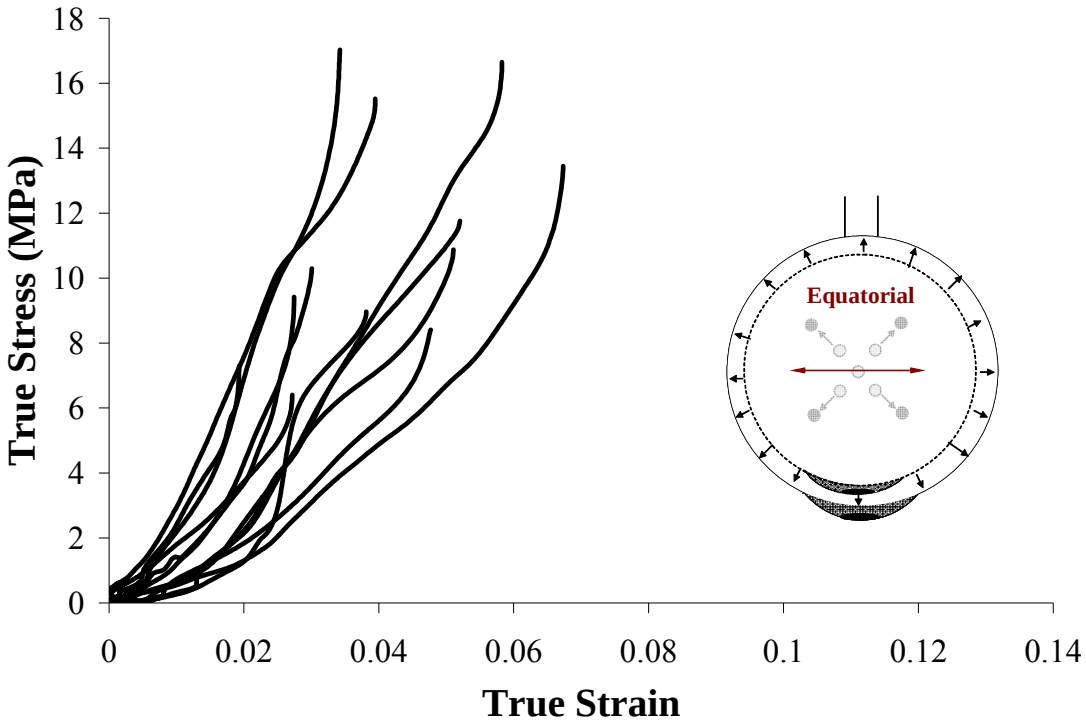

Figure 7: Stress-strain curve responses in the equatorial direction of 12 eye rupture tests.

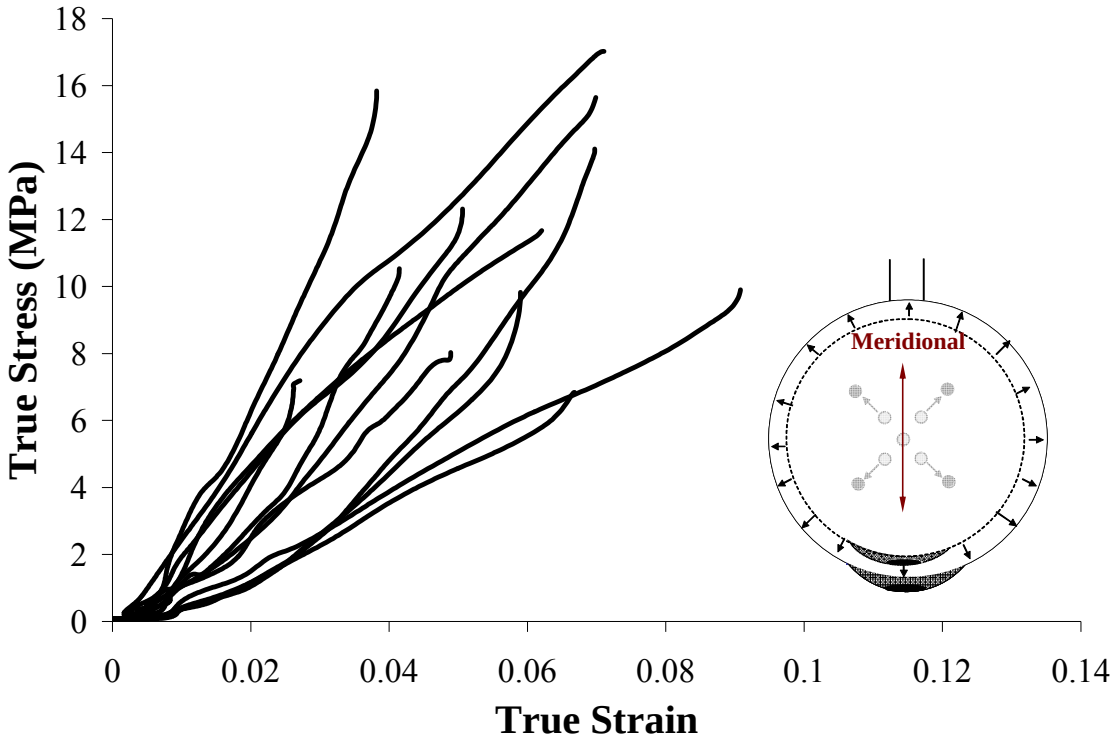

Figure 8: Stress-strain curve response in the meridional direction of 12 eye rupture tests.

Table 2: True stress and True strain results for 12 human eyes.

Test	Maximum Equatorial Strain	Maximum Meridional Strain	Maximum Stress (MPa)	Time to Rupture (ms)	Thickness (mm)
1	0.0274	0.0590	12.15	21.23	0.46
2	0.0301	0.0415	12.63	23.80	0.56
3	0.0272	0.0673	6.84	26.13	0.81
4	0.0381	0.0908	10.31	28.07	0.59
5	0.0343	0.0724	17.03	28.67	0.47
6	0.0511	0.0506	15.16	28.77	0.51
7	0.0673	0.0697	20.37	29.33	0.62
8	0.0582	0.0382	20.20	29.77	0.44
9	0.0395	0.0709	18.16	31.47	0.54
10	0.0193	0.0489	8.08	37.33	0.85
11	0.0524	0.0639	17.30	38.97	0.49
12	0.0478	0.0262	8.41	45.87	0.57
Average	0.0410	0.0580	13.89	30.78	0.58
Standard Deviation	0.0140	0.0180	4.81	6.87	0.13

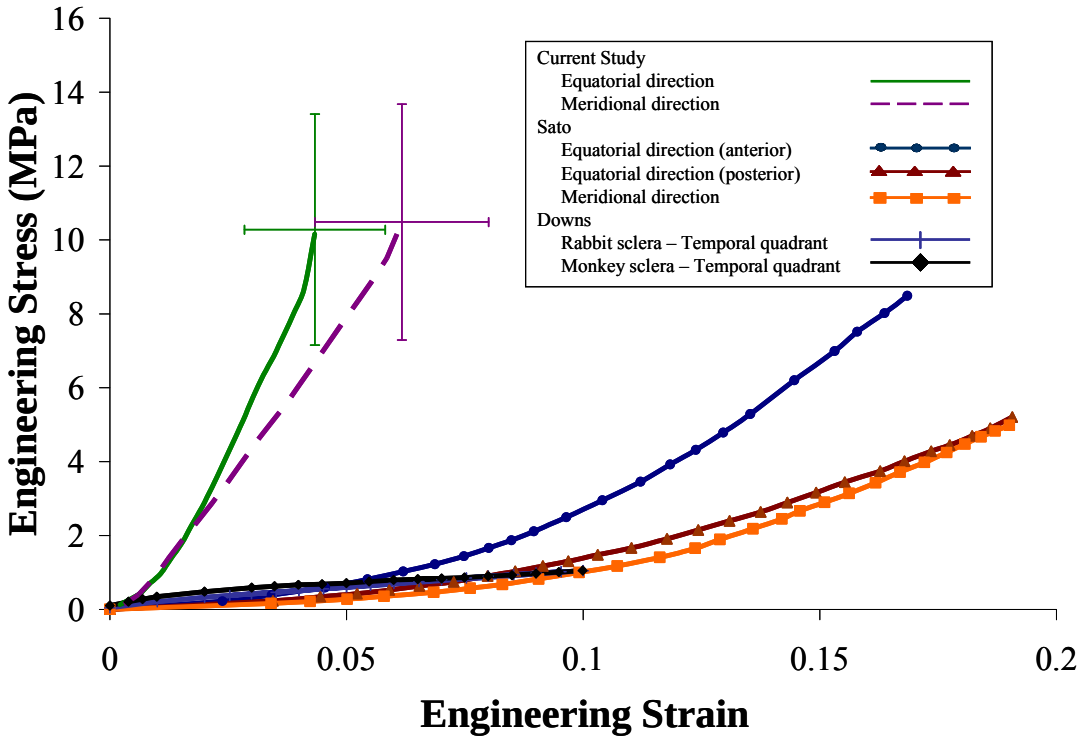

Figure 9: Comparison of previous stress-strain curves to current study.

DISCUSSION

Although the tests performed by Sato (1970) were both static and uniaxial, general trends of rate dependence and directional dependence between the current study and the previous study were determined. Interestingly, both test series showed that the equatorial direction has a larger stiffness than the meridional direction, which concludes that the sclera is an anisotropic material (Figure 9). In terms of rate dependence, the dynamic tests showed much lower strain at equivalent stress values when compared to the static tests. Downs et al. characterized the material properties of the sclera for rabbit and monkey in four quadrants surrounding the optic nerve (Downs, 2003). The results showed that there were no detected differences in the stress-strain curves for 0-10% strain between the quadrants for monkey sclera. However, differences were detected by quadrant for rabbit sclera at strains below 4 percent. The test series performed by Downs resembles that of Sato because of the uniaxial loading mode and the slow strain rate (1 percent/s). The current test series was able to determine directional components of stress

and strain, as well as, determine stress and strain at a higher strain rate (150 percent/s) to more accurately represent the speed of an impact with an airbag. These comparisons of engineering stress and strain helped to validate the rate dependence and the directional dependence of the sclera and conclude that the sclera is both anisotropic and viscoelastic (Yamada, 1970; Uchio, 1999).

In order to characterize any difference between stress and strain at the optical marker location and the rupture location a comparison was performed. Three tests that ruptured close to the optical markers (Test 5, 11 and 12) and three tests that ruptured away from the optical markers (Test 1, 6, and 8) were compared graphically (Figure 10), and were found to produce similar responses.

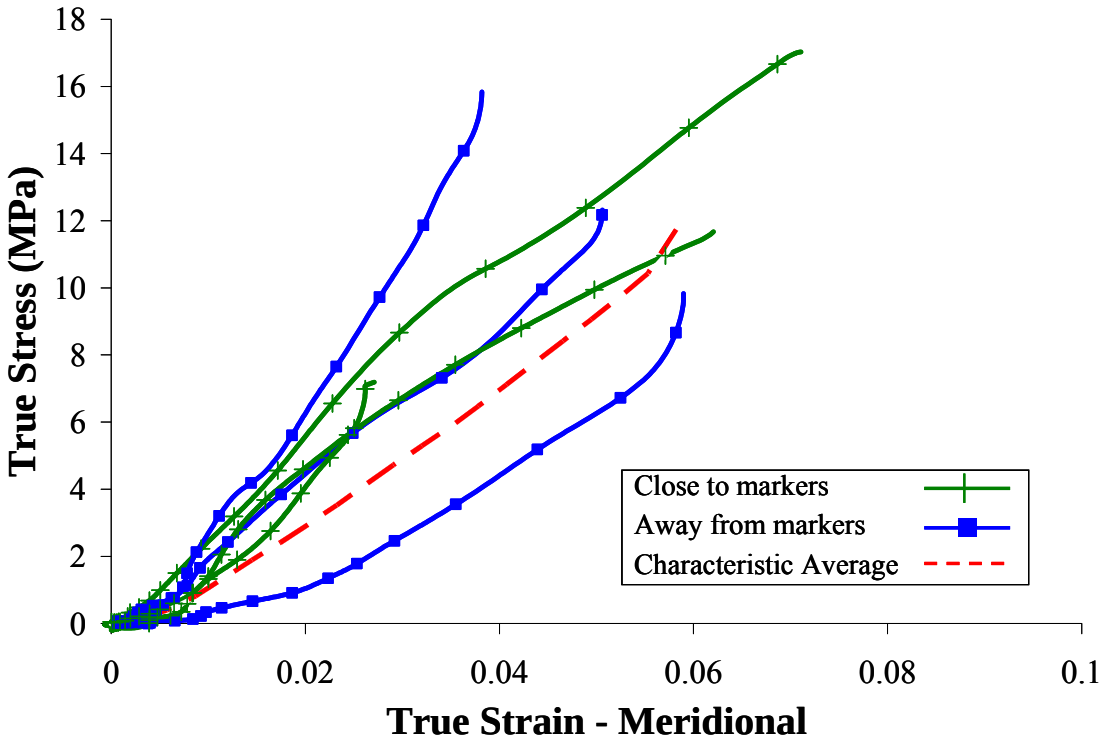

Figure 10: Stress and strain comparison for tests with rupture close to and away from optical markers in the meridional direction.

As stated in previous literature, the time after death prior to testing does not correlate to the degradation of the corneo-scleral shell with an R^2 value of 0.14 (Kennedy, 2004). The tissue breaks down very slowly and is sensitive to freeze-thaw cycles. Since the tissue was never frozen and was stored in refrigerated saline, the integrity of the globe

was maintained prior to testing. An analysis was done that showed no correlation between the rupture pressure and the time from the harvest to the test date which produced an R^2 value of 0.07.

It was also noted that the direction of the rupture (equatorial or meridional) was not correlated to an increase or decrease in stress or strain. There were not enough tests that differed with rupture direction to perform a full statistical analysis to determine a correlation with stress and strain. However, the one test that did rupture along the meridian resulted in 15.16 MPa, 0.0511, and 0.0506 for the maximum true stress, equatorial strain and meridional strain. In the case of rupture location, there was one test with a rupture location at the optical markers while the remainder of the eyes had rupture locations that did not travel through the optical markers. This test produced values of 17.03 MPa, 0.0343, and 0.0724 for maximum stress, equatorial strain and meridional strain respectively.

Limitations

In this study, thickness measurements were taken using a high accuracy laser but even with this precise measurement, variability is still present. Because the thickness measurements were taken at the location of the markers rather than the rupture location, the results represent sub-failure data. The thickness varies across the eye and therefore could only be approximated. It is especially difficult to obtain the thickness directly at the optical markers as the local tissue deforms, curls, or is missing post-test. Because of the placement of the thickness in the stress equation it becomes imperative to have an accurate measurement.

When determining the true strain of the human eye, two limitations were the accuracy with which the software tracked the optical markers and the curvature of the eye. The average tracking error for the strain calculations was found to be 0.54%. Another consideration lies within the difference between a two dimensional strain calculation and a three dimensional calculation. The optical markers were created from a stamp to ensure that they were no more than 3.81 mm apart. The curvature of the eye was compared to

the assumption of an in-plane calculation. For the twelve human eyes tested, the average error when using the two dimensional calculation was 1.23%.

ACKNOWLEDGEMENTS

The authors would like to acknowledge the United States Army Aeromedical Research Laboratory for their support of this research program. The authors would also like to acknowledge the Virginia Tech - Wake Forest Center for Injury Biomechanics for funding the tissue testing.

REFERENCES

Ahearne, M., Yang, Y., Then, K. Y., et al. (2007). An indentation technique to characterize the mechanical and viscoelastic properties of human and porcine corneas. **Annals of Biomedical Engineering 35**(9): 1608-1616.

Battaglioli, J. L. and Kamm, R. D. (1984). Measurements of the compressive properties of scleral tissue. **Investigative Ophthalmology and Visual Science 25**: 59-65.

Bryant, M. R. and Mcdonnell, P. J. (1996). Constitutive laws for biomechanical modeling of refractive surgery. **Journal of Biomechanical Engineering 118**: 473-481.

Downs, C. J., Suh, F. J.-K., Thomas, K. A., et al. (2003). Viscoelastic characterization of peripapillary sclera: material properties by quadrant in rabbit and monkey eyes. **Journal of Biomechanical Engineering 125**: 124-131.

Duma, S. M. and Crandall, J. R. (2000). Eye injuries from airbags with seamless module covers. **The Journal of Trauma 48**(4): 786-789.

Duma, S. M., Jernigan, M. V., Stitzel, J. D., et al. (2002). The effect of frontal air bags on eye injury patterns in automobile crashes. **Arch Ophthalmol 120**(11): 1517-22.

Hanna, K. D., Jouve, F. E., Waring, G. O., et al. (1989). Computer simulation of arcuate and radial incisions involving the corneoscleral limbus. **Eye 3**: 227-239.

Kennedy, E. A., Inzana, J. A., Mcnally, C., et al. (2007). Development and validation of a synthetic eye and orbit for estimating the potential for globe rupture due to specific impact conditions. **Stapp Car Crash Journal 51**: 381-400.

Kennedy, E. A., Ng, T. P., Mcnally, C., et al. (2006). Risk functions for human and porcine eye rupture based on projectile characteristics of blunt objects. **Stapp Car Crash Journal 50**: 651-671.

Kennedy, E. A., Voorhies, K. D., Herring, I. P., et al. (2004). Prediction of severe eye injuries in automobile accidents: static and dynamic rupture pressure of the eye. **Association for the Advancement of Automotive Medicine 48**: 165-179.

Kisielewicz, L. T., Kodama, N., Ohno, S., et al. (1998). "Numerical prediction of airbag caused injuries on eyeballs after radial keratotomy." **SAE International Congress and Exposition**.

Kuhn, F., Collins, P., Morris, R., et al. (1994). Epidemiology of motor vehicle crash-related serious eye injuries. **Accident Analysis and Prevention 26**(3): 385-390.

Lessley, D., Crandall, J., Shaw, G., et al. (2004). A normalization technique for developing corridors from individual subject responses. **SAE Technical Paper Series 1**: 1-11.

Mcgwin, G., Xie, A. and Owsley, C. (2005). Rate of eye injury in the united states. **Archives of Ophthalmology 123**: 970-976.

Nash, I. S., Greene, P. R. and Foster, C. S. (1982). Comparison of mechanical properties of keratoconus and normal corneas. **Exp Eye Res 35**: 413-423.

Parver, L. M. (1986). Eye trauma: the neglected disorder. **Archives of Ophthalmology 104**: 1452-1453.

Sawusch, M. R. and Mcdonnell, P. J. (1992). Computer modeling of wound gape following radial keratotomy. **Refractive and Corneal Surgery 8**: 143-145.

Stitzel, J. D., Duma, S. M., Cormier, J. M., et al. (2002). A nonlinear finite element model of the eye with experimental validation for the prediction of globe rupture. **Stapp Car Crash Journal 46**: 81-102.

Uchio, E., Ohno, S., Kudoh, J., et al. (1999). Simulation model of an eyeball based on finite element analysis on a supercomputer. **British Journal of Ophthalmology 83**: 1106-1111.

Wray, W. O., Best, E. D. and Cheng, L. Y. (1994). A mechanical model for radial keratotomy: toward a predictive capability. **Journal of Biomechanical Engineering 116**: 56-61.

Yamada, H. and Evans, F. G. (1970). Strength of biological materials. Baltimore, Williams & Wilkins.

CHAPTER 3: INTRAOCULAR PRESSURE DURING HIGH SPEED PROJECTILE IMPACTS

ABSTRACT

Objectives: To determine intraocular pressure during high speed projectile impact to eyes.

Methods: A pneumatic cannon was used to impact eyes with a variety of projectiles at multiple velocities. The internal eye pressure was measured with a small pressure sensor inserted into the eye through the optic nerve. A total of 49 tests were performed on 12 porcine eyes to measure intraocular pressure during a high speed projectile impact with a range of velocities from 4.39 m/s to 64.92 m/s. The projectiles selected for the test series included a 6.35 mm diameter metal ball, a 9.25 mm diameter aluminum rod, and an 11.16 mm diameter aluminum rod.

Results: A range of internal eye pressures were produced that varied from 1256 mmHg (24.3 psi) to 22843 mmHg (442 psi). The intraocular pressure results varied with water stream velocity and nozzle diameter. A total of 49 impacts were conducted with 12 porcine eyes that resulted in zero globe rupture.

Conclusions: Intraocular pressure was measured in eyes for high speed projectile impacts. The results will help to characterize the response of the eye for projectile impacts that do not cause globe rupture.

INTRODUCTION

Blindness due to ocular trauma is a significant problem in the United States. Over 1.9 million people suffered from eye injuries that required treatment in the United States in 2001.[1] The most likely sources of eye injuries include automobile accidents[2-7], sports related impacts[8, 9], consumer products, and military combat.[10] Approximately 500,000 years of lost eyesight occur in the United States each year.[11] These injuries are expensive to treat given the estimated annual cost associated with adult vision problems in the United States is $51.4 billion.[12, 13]

In order to predict and consequently prevent these eye injuries for various impact scenarios, previous research has investigated eye injuries for projectile impacts with known projectile characteristics[8, 14, 15]. Duma et al. included diameter, mass, velocity, kinetic energy, and normalized energy in their study to determine the best predictor for ocular injury. A logistic regression was used and concluded that normalized energy was the most significant predictor of injury type and tissue lesion. Values were reported for 50% injury risk of corneal abrasion, lens dislocation, hyphema, retinal damage, and globe rupture. This presents a useful tool for predicting eye injuries when the projectile characteristics are known, however there are many cases of blunt trauma when these variables are unknown and the measurement of intraocular pressure is preferred.

A previous study determined the rupture pressure for human eyes[16]. Internal pressure was dynamically induced into the eye using a drop tower pressurization system. The internal eye pressure was measured with a small pressure sensor inserted into the eye through the optic nerve. The high rate pressurization resulted in a mean rupture pressure of 7276 ± 2175 mmHg (141 ± 42.1 psi). Although this study succeeded in providing pressure results for the most severe of eye injuries, data is needed for additional eye injuries that are more frequent in occurrence.

Studies have reported the injury risk for projectile impacts to the globe but have not reported the corresponding intraocular pressure. In addition, intraocular pressure for globe rupture has also been study presented. Therefore, the purpose of the current study is to determine intraocular pressure during high speed projectile impacts to eyes.

METHODS

Blunt impacts to porcine eyes were performed with a custom pressure system that was built to determine internal eye pressure. The test setup consisted of a pneumatically powered cannon with a pressure regulator to control the velocity of the projectile, a solenoid valve, and three changeable barrels (Figure 11). In order to ensure a direct hit to the cornea, a placement guide was constructed to act as a support for the eye that did not

constrain movement. In preparation for each test, the porcine eye was instrumented with a needle connected to a water chamber that was filled to produce an initial intraocular pressure of 14.95 mmHg (8 inH_2O) to represent normal physiologic pressure. The optic nerve and needle were secured with a clamping system.

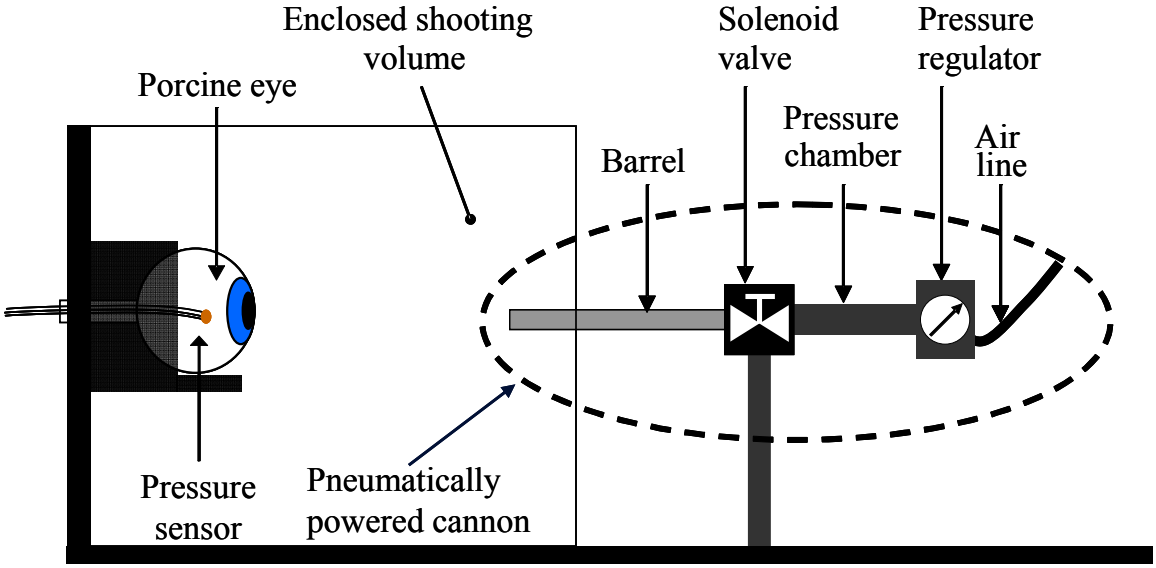

Figure 11: Experimental testing was performed used a pneumatically powered cannon in an enclosed shooting volume to impact porcine eyes.

Measurements of the internal pressure of the porcine eye were acquired using an *in situ* pressure sensor. This small pressure sensor (Precision Measurement Company, Model 060, Ann Arbor, MI) was inserted into the eye through the optic nerve. The pressure transducer was rated for a range of 0-25877 mmHg (0-500 psi) and had a frequency response of 10 kHz which were both sufficient for this application.

A series of impact tests were conducted using porcine eyes with three rigid projectiles at a range of velocities. For each test the barrel size was chosen and the pressure regulator was set to produce a chosen velocity. The projectiles selected for the test series included a 6.35 mm diameter metal ball, a 9.25 mm diameter aluminum rod, and an 11.16 mm diameter aluminum rod, with impact velocities ranging from 4.26 m/s – 64.92 m/s (Figure 12). In order to capture each impact, high speed video and data acquisition were used. A Phantom v9.1 camera (Vision Research, Wayne, NJ) captured video at 3902

frames per second with a resolution of 960 x 480, while the data acquisition system (DAS) collected data at 50 kHz. The pressure sensor measured internal eye pressure throughout the event and was filtered using CFC 600 Hz.

Figure 12: Relative size differences of the three projectiles compared to a penny (Left to Right: penny, large aluminum rod, small aluminum rod, small metal ball).

High speed video was utilized to track the velocity of each projectile impact. Normalized energy of a projectile was defined as the kinetic energy divided by the cross-sectional area of the object. This calculation included the object's mass, velocity and cross-sectional area[14]. Projectile velocity, normalized energy and internal eye pressure were reported for each test.

RESULTS

A total of 49 projectile impact tests on 12 porcine eyes were designed to produce a range of intraocular pressures in order to represent a variety of eye injury severities. Internal eye pressures varied from 1257 mmHg to 22843mmHg (24.3 psi - 442 psi) depending on the speed and size of the projectiles. It should be noted that there were some recorded intraocular pressures that exceeded the rupture pressure threshold for the human eye. High speed video was used to evaluate the projectile trajectory and to provide a measurement of projectile velocity which resulted in a range of 14.4 m/s to 64.92 m/s (Figure 13). The tests produced normalized energy levels that varied from 538 J/m^2 to 71,563 J/m^2. Internal eye pressure, normalized energy and velocity for each test were reported (Table 3, Table 4, Table 5).

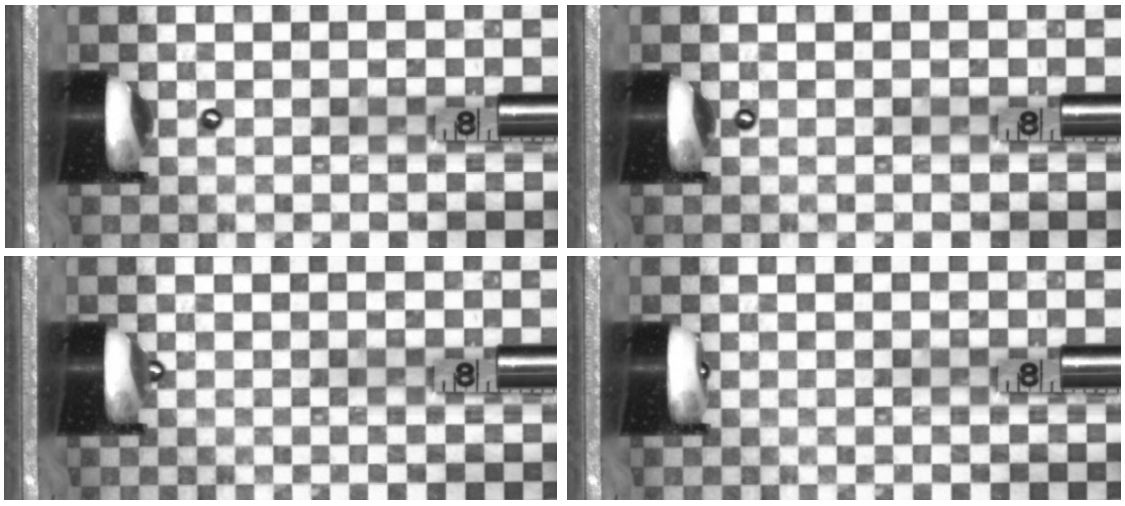

Figure 13: High speed video documentation of a test with the 6.35 mm metal ball projectile.

Table 3: Internal eye pressure, normalized energy and velocity results for the small aluminum rod projectile. (mass = 3.61 g, diameter = 9.25 mm)

Test Number	Peak Internal Eye Pressure (mmHg)	Peak Internal Eye Pressure (psi)	Normalized Energy (J/m^2)	Velocity (m/s)
1	2662	51.47	1553	7.42
2	11442	221.26	19667	26.39
3	17634	340.98	14999	23.05
4	16623	321.44	23082	28.59
5	19838	383.59	32813	34.09
6	3898	75.38	1667	7.68
7	8709	168.39	5748	14.27
8	11383	220.11	8741	17.60
9	16550	320.03	16526	24.19
10	17388	336.23	26770	30.79
11	17198	332.56	16526	24.19
12	12449	240.73	9868	18.69
13	8186	158.29	6640	15.34
14	3992	77.18	1220	6.57
15	21794	421.42	30730	32.99

Table 4: Internal eye pressure, normalized energy and velocity results for the large aluminum rod projectile. (mass = 5.19 g, diameter = 11.16 mm)

Test Number	Peak Internal Eye Pressure (mmHg)	Peak Internal Eye Pressure (psi)	Normalized Energy (J/m^2)	Velocity (m/s)
1	2263	43.75	1424	7.15
2	7913	153.02	8627	17.60
3	13195	255.15	6605	15.40
4	19368	374.51	16310	24.19
5	8019	155.06	3344	10.95
6	1919	37.11	538	4.39
7	8329	161.07	3370	11.00
8	14509	280.56	8627	17.60
9	22385	432.85	16183	24.10
10	9456	182.85	4439	12.62
11	4398	85.04	1015	6.04
12	15008	290.20	7523	16.43
13	22843	441.70	16310	24.19

Table 5: Internal eye pressure, normalized energy and velocity results for the small metal ball projectile. (mass = 1.02 g, diameter = 6.35 mm)

Test Number	Peak Internal Eye Pressure (mmHg)	Peak Internal Eye Pressure (psi)	Normalized Energy (J/m^2)	Velocity (m/s)
1	1824	35.27	1485	9.35
2	6597	127.56	7421	20.89
3	9162	177.16	13897	28.59
4	13859	267.99	29686	41.79
5	16795	324.77	41630	49.49
6	18935	366.14	57748	58.28
7	5457	105.52	6661	19.79
8	8943	172.93	13897	28.59
9	12536	242.41	29686	41.79
10	1255	24.27	1311	8.78
11	17161	331.84	71563	64.88
12	8832	170.78	17289	31.89
13	12987	251.12	29686	41.79
14	1832	35.43	1152	8.23
15	6300	121.82	6661	19.79
16	16130	311.90	43501	50.59
17	18377	355.35	55589	57.18
18	13231	255.84	27925	40.53
19	5957	115.18	7364	20.81
20	9099	175.95	14870	29.58
21	16349	316.14	41630	49.49

COMMENT

Duma et al. were interested in finding the best predictor of injury when impacting an eye with a projectile[14]. Five projectile characteristics were analyzed and results showed that kinetic energy and normalized energy were in the top group of good predictors. For this reason the current study investigated a correlation between intraocular pressure and kinetic energy and intraocular pressure and normalized energy. It was found that the least squares regression showed a good fit (R^2=0.83) for the correlation between internal eye pressure and kinetic energy using a curve fit analysis (Figure 14). This fit proved to be better than that between normalized energy and intraocular pressure. This could be expected because of the influence of area within the normalized energy calculation. In previous research, normalized energy has been shown to be the most significant predictor of injury[14]. Although utilizing normalized energy decreased the goodness of fit slightly, there was a significant gain in the ability to predict injury when looking at normalized energy[14]. The same study was able to derive injury risk functions for corneal abrasion, hyphema, retinal damage, lens dislocation and globe rupture as a function of normalized energy which adds to the benefit of using normalized energy. These risk functions could be utilized in future studies to determine the risk of injury for projectile impacts.

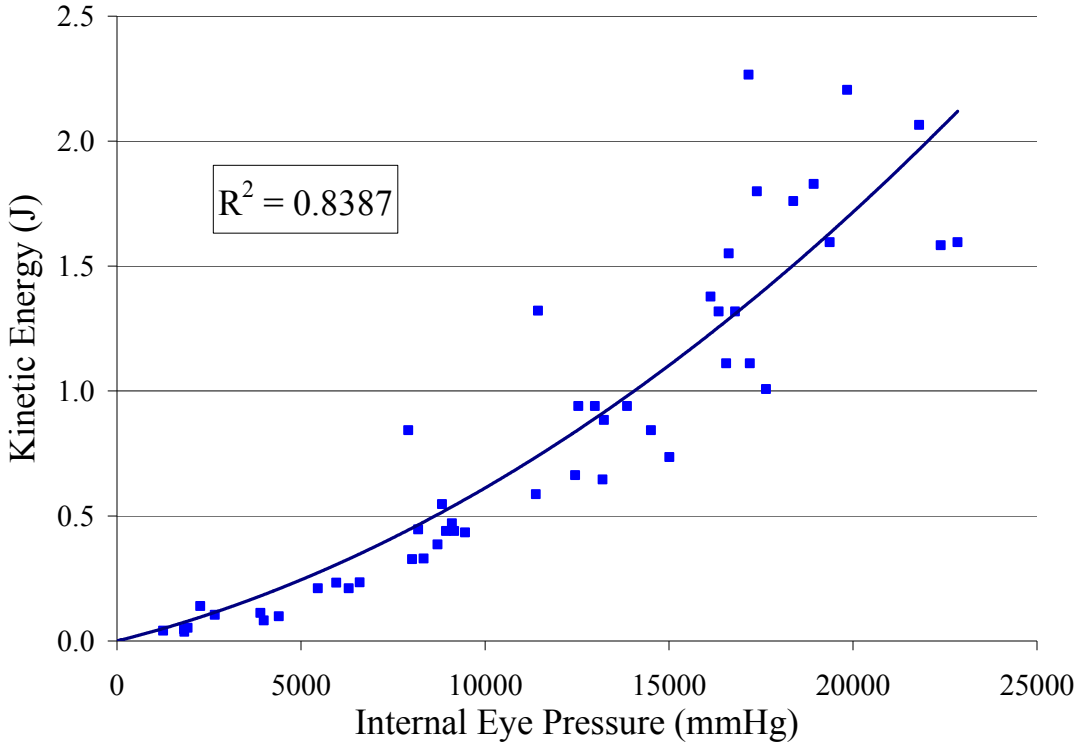

Figure 14: Correlation between internal eye pressure and kinetic energy.

The influence of projectile size was investigated by expanding the range of internal eye pressure (Figure 15). By separating the curve fit lines by projectile type it was clear that there was a trend. As the projectile size decreased, the normalized energy increased when considering a similar internal eye pressure. This trend is less apparent when looking at the points within the chosen threshold of 11894.43 mmHg (230 psi).

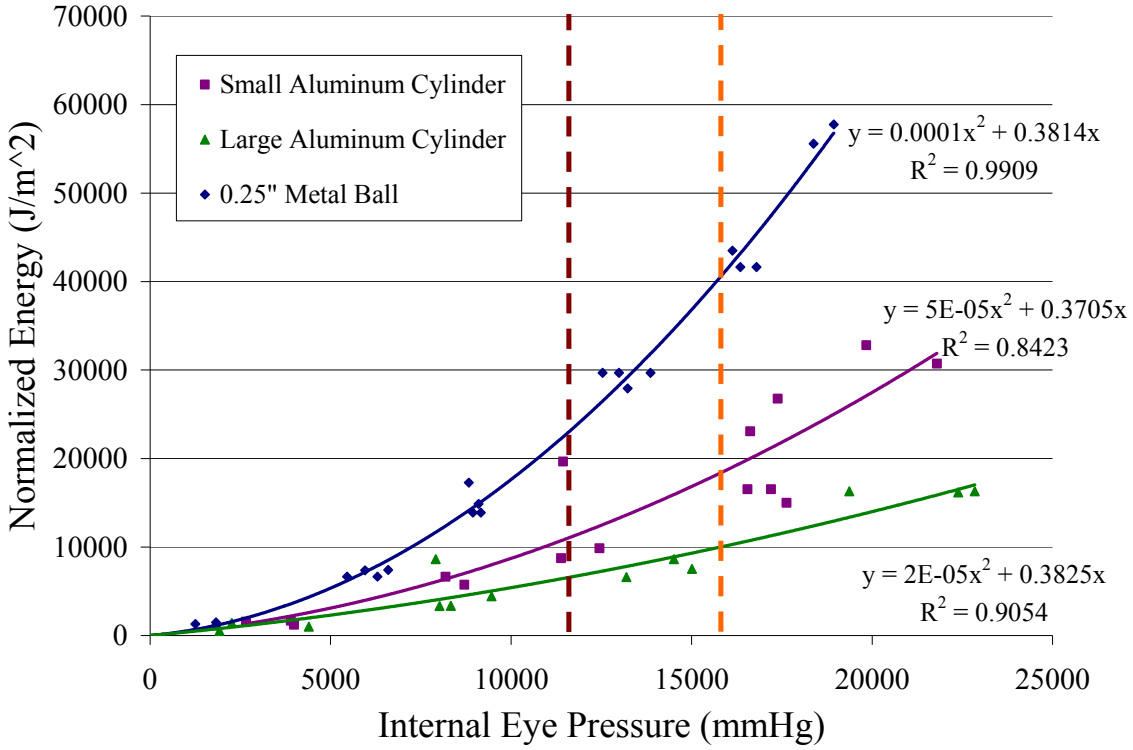

Figure 15: Correlation between internal eye pressure and normalized energy at full range with the human rupture pressure threshold at 11894 mmHg and the porcine rupture pressure threshold at 16342 mmHg.

Twelve porcine eyes were procured from Animal Technologies (Tyler, TX) and stored in saline for the current test series. They were kept refrigerated for a maximum of 14 days prior to testing. Because the tissue was never exposed to a freeze-thaw cycle and was stored in refrigerated saline, the integrity of the globe was preserved before the testing. A previous study showed the lack of correlation between rupture pressure and the time from the test date to harvest which resulted in an R^2 value of 0.06[4].

The effect of varied location of the pressure sensor inside the eye was considered. Previously conducted research inserted multiple sensors into one eye to compare the response of two identical pressure sensors in different locations during a dynamic event[16]. The response showed that regardless of the location of the sensors the pressure output was the same. This analysis was assumed to be relevant for the current test series.

The use of porcine eyes as a surrogate for human eyes is a limitation in this study. In previous literature, researchers have used many different surrogates for experimental testing. Because of the anatomical and mechanical similarities between porcine and human eyes and the additional availability, porcine eyes were utilized for the current study. Due to the difference in rupture pressure between porcine and human eyes, there were some impacts that exceeded the human rupture pressure threshold but did not result in a rupture. Bisplinghoff et al. reported average rupture pressure of human eyes as 7275 mmHg (141 psi) with a maximum pressure of 11925 mmHg (231 psi), while Kennedy et al. reported average porcine rupture pressure as 12256 mmHg (237 psi) with a maximum pressure of 16342 mmHg (316 psi)[16, 17]. The maximum pressures for both human and porcine eyes were used as the thresholds shown in Figure 15.

The correlation between internal eye pressure and normalized energy from this study has great potential to be used for future applications. For impact situations where the normalized energy in unavailable this approach will allow for the calculation of injury risk. Possible applications could include an advanced headform with an instrumented synthetic eye to read pressure during experimental impacts. Also, eye injuries from water stream impacts are of particular interest to water park and water toy designers. Results from this study can provide the data needed to affect the design of consumer products and their safety.

ACKNOWLEDGEMENTS

The authors would like to acknowledge the Virginia Tech - Wake Forest Center for Injury Biomechanics for funding this research.

REFERENCES

1. McGwin G, Xie A, Owsley C. Rate of eye injury in the United States. *Arch Ophthalmol.* 2005;123:970-976.

2. Duma SM, Jernigan MV, Stitzel JD, et al. The effect of frontal air bags on eye injury patterns in automobile crashes. *Arch Ophthalmol.* Nov 2002;120(11):1517-1522.

3. Fukagawa K, Tsubota K, Kimura C, et al. Corneal endothelial cell loss induced by air bags. *Ophthalmology.* 1993;100(12).

4. Kennedy EA, Voorhies KD, Herring IP, Rath AL, Duma SM. Prediction of severe eye injuries in automobile accidents: static and dynamic rupture pressure of the eye. *Association for the Advancement of Automotive Medicine.* 2004;48:165-179.

5. Kisielewicz LT, Kodama N, Ohno S, Uchio E. Numerical prediction of airbag caused injuries on eyeballs after radial keratotomy. Paper presented at: SAE International Congress and Exposition, 1998; Detroit, Michigan.

6. Duma SM, Crandall JR. Eye injuries from airbags with seamless module covers. *The Journal of Trauma.* 2000;48(4):786-789.

7. Duma SM, Kress TA, Porta DJ, et al. Airbag-induced eye injuries: A report of 25 cases. *The Journal of Trauma.* 1996;41(1):114-119.

8. Kennedy EA, Ng TP, McNally C, Stitzel JD, Duma SM. Risk functions for human and porcine eye rupture based on projectile characteristics of blunt objects. *Stapp Car Crash Journal.* 2006;50:651-671.

9. Vinger PF, Duma SM, Crandall J. Baseball hardness as a risk factor for eye injuries. *Arch Ophthalmol.* Mar 1999;117(3):354-358.

10. Heier JS, Enzenauer RW, Wintermeyer SF. Ocular injuries and diseases at a combat support hospital in support of Operations Desert Shield and Desert Storm. *Archives of Ophthalmology.* 1993;111:795-798.

11. United States Eye Injury Registry. *Eye trauma: Epidemiology and prevention* [http://www.useironline.org/Prevention.htm. Accessed March 11, 2009.

12. Frick KD, Gower EW, Kempen JH, Wolff JL. Economic impact of visual impairment and blindness in the United States. *Arch Ophthalmol.* Apr 2007;125(4):544-550.

13. Rein DB, Zhang P, Wirth KE, et al. The economic burden of major adult visual disorders in the United States. *Arch Ophthalmol.* Dec 2006;124(12):1754-1760.

14. Duma SM, Ng TP, Kennedy EA, Stitzel JD, Herring IP, Kuhn F. Determination of significant parameters for eye injury risk from projectiles. *Journal of Trauma.* 2005(59):960-964.

15. Kennedy EA, Inzana JA, McNally C, et al. Development and validation of a synthetic eye and orbit for estimating the potential for globe rupture due to specific impact conditions. *Stapp Car Crash Journal.* October 2007 2007;51:381-400.

16. Bisplinghoff JA, McNally C, Duma SM. High rate internal pressurization of human eye to predict globe rupture. *Arch Ophthalmol.* April 2009.

17. Kennedy EA, Voorhies KD, Herring IP, Rath AL, Duma SM. Prediction of severe eye injuries in automobile accidents: static and dynamic rupture pressure of the eye. *Annu Proc Assoc Adv Automot Med.* 2004;48:165-179.

CHAPTER 4: EYE INJURY RISK FROM WATER STREAM IMPACT

ABSTRACT

Objectives: To determine the eye injury risk of water stream impacts with a variety of velocities and nozzle diameters that are commonly found in toy water guns and water parks.

Methods: Water streams were developed using a customized pressure system to impact porcine eyes. The water velocity was varied between 2 m/s and 17.4 m/s while using three nozzle diameters (3.18 mm, 6.35 mm and 9.53 mm). The internal eye pressure was measured with a small pressure sensor inserted into the eye through the optic nerve and then correlated to injury risk using previous literature.

Results: A total of 73 water stream impact tests were designed to impact the eye with different nozzle sizes at a range of velocities. The experimental water stream impacts created a range of intraocular pressures from 166 mmHg to 6826 mmHg (3.21psi to 132 psi). The tests resulted in 0% risk of injury for hyphema, lens dislocation, retinal damage and globe rupture.

Conclusions: Intraocular pressures were measured in order to calculate injury risk for water stream impacts. It was determined that there was 0% risk of injury for the nozzle diameters and water velocities chosen. These results help to determine thresholds to aid in the design of interactive water displays and water toys.

INTRODUCTION

Ocular trauma that leads to blindness is a significant expense in the United States. This is evident in the estimated $51.4 billion spent on adult vision problems each year[1, 2]. The most likely sources of eye injuries include sports related impacts[3, 4], automobile accidents[5-10], consumer products, and military combat[11]. Out of the 1.9 million total eye injuries in the country, more than 600,000 sports injuries occur each year and 40,000 of them require emergency care[12, 13]. Considering that each year approximately 500,000 years of eyesight are lost, eye injuries are a serious problem in the U.S.[14]

Concern has been raised by water park and toy designers about the potential danger of water stream eye injuries. The impact of a high-velocity water stream on the globe has not been previously quantified. Such pressurized water streams can be found in children's water toys, squirt guns, and interactive water fountains. As the velocity of these water streams increases, product capabilities, and therefore popularity, likewise increase. Interactive water fountains are found in public areas and water parks throughout the country. These attractions feature synchronized streams of water, typically directed vertically from nozzles in the ground which have the capability to cause an eye injury. However, the increasing popularity of these fountains has not been matched by appropriate regulation. The primary focus of the current legislation is centered on the filtration system and prevention of spread of bacterial infection. This concern has taken attention away from potential mechanical ocular injuries due to a high-velocity water stream. Nozzle size and maximum velocity are a critical part of the performance of an interactive water fountain. However, until relationships between these factors and injury have been established, it is hard to place numerical guidelines on their design. Documented cases of high-velocity water-induced eye injuries confirm the potential danger of these water blasts. Many of the reported incidents occurred in the workplace and involve pressure washers, agricultural irrigation sprinklers, or fire hoses.

Although studies of water-induced eye injuries have not been conducted on human eyes, animal studies have linked high-velocity water streams to ocular damage. Fish (*Oncorhynchus tshawytscha*) exposed to submerged water streams at velocities ranging from 12 to 20 m/s were examined for injury. Nearly half of all fish suffered eye injuries (bulged, hemorrhaged, or missing) at velocities of 17 m/s and above[15]. In a similar study, fish were released at velocities from 0 to 21 m/s and the authors found velocity to be positively correlated to severity of injury[16]. Minor severity was noted when there was a visible injury that had no threat to life and major severity was noted when the injury was a threat to life and persisted throughout time. The deformable nature of fluids has proved to be harmful, especially without transfer of momentum to the orbital margin, as occurs when a large solid object is targeted toward the eye.

The purpose of the current study is to first evaluate the relationship between intraocular pressure and injury risk for water impacts and second to calculate injury risk for hyphema, lens dislocation, retinal damage and globe rupture for each experimental water impact.

METHODS

Water stream impacts to porcine eyes were performed with a custom pressure system that was built to measure internal eye pressure and the velocity of the water stream. The pressure system consisted of a pressure regulator to control the water velocity, a solenoid valve, and three changeable nozzles (Figure 16). A placement guide was added to the system to ensure that the water stream hit the cornea directly and that the porcine eye was free to move without constraint. Preparation before each test involved connecting the eye to a water chamber to produce an initial intraocular pressure of 14.95 mmHg (8 inH_2O). This was accomplished by inserting a needle through the optic nerve along with a small pressure sensor. A clamping system was used to secure the optic nerve, needle and pressure sensor.

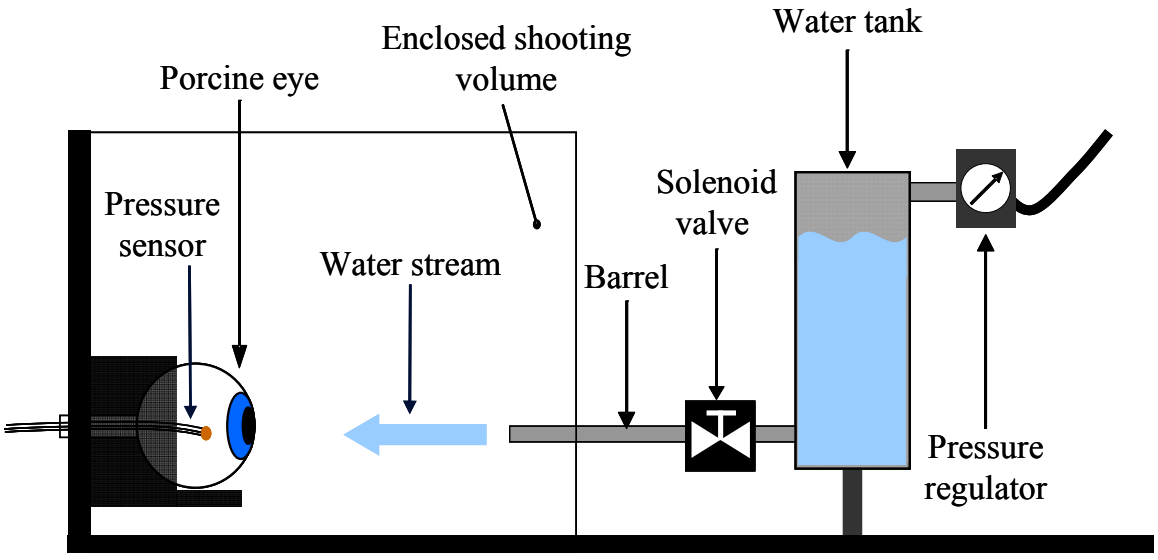

Figure 16: Water stream system used to impact porcine eyes.

Measurements of the internal pressure of the porcine eye were acquired using an *in situ* pressure sensor. This small pressure sensor (Precision Measurement Company, Model 060, Ann Arbor, MI) was inserted into the eye through the optic nerve. The pressure transducer was rated for a range of 0-25877.1 mmHg (0-500 psi) and had a frequency response of 10 kHz which were both sufficient for this application.

A series of water impact tests were conducted using three nozzle diameters at a range of velocities. For each test the nozzle size was chosen and the pressure regulator was set to produce a chosen velocity. The different barrels were used to create three stream sizes (3.18mm, 6.35mm, and 9.53mm) to investigate the influence of stream diameter on injury risk. In order to capture each impact, high speed video and data acquisition were used. A Phantom v9.1 camera (Vision Research, Wayne, NJ) captured video at 3902 frames per second with a resolution of 960 x 480, while the data acquisition system (DAS) collected data at 50 kHz. The pressure sensor measured internal eye pressure throughout the event and was filtered using CFC 600 Hz. The pressure transducer data and the high-speed video were used to determine the internal eye pressure and the velocity of the water stream. The variety of nozzle diameters and velocities created a data set that reflected the settings the would be produced by an interactive water display.

In order to analyze the current dataset two previous studies were used to relate intraocular pressure and injury risk. The first study reported the correlation between intraocular pressure and normalized energy (Chapter 3). A second study determined injury risk as a function of normalized energy for hyphema, lens dislocation, retinal damage and globe rupture[3, 17]. From these data, intraocular pressure could then be related to injury risk for water impacts.

Chapter 3 reported intraocular pressure and normalized energy for projectile impacts. Normalized energy and the measured internal eye pressure from the previous study were correlated using a curve fit analysis. A maximum pressure of 11894 mm Hg (230 psi) was chosen based on the peak rupture pressure of human eyes reported in previous literature[18]. A second order polynomial curve fit was used to determine the equation to

correlate the two parameters (Equation 1) with an R^2 value of 0.6062. This analysis produced an equation that was then used to relate internal eye pressure to normalized energy for the water stream impacts.

$$y = 0.2029 \cdot x^2 + 21.923 \cdot x. \quad \text{Eq. 1}$$

Previously developed injury risk curves for hyphema, lens dislocation, retinal damage and globe rupture were applied to the calculated normalized energy to determine injury risk for the water stream impacts (Table 6)[3, 17]. Given the calculated normalized energy values for each water stream impact, the injury risk for each eye injury was determined using the risk function coefficients determined from published research. A general form of the injury risk function (Equation 2) was used to express a relationship between normalized energy (x) and the probability of injury. Parameters "a" and "b" refer to constants that have been determined by previous research through logistic regression and are unique to the specific predictor.

$$\text{Probability of Injury (\%)} = \frac{1}{1+e^{a-bx}} \quad \text{Eq. 2}$$

Table 6: Injury risk function coefficients from published research.

	Parameter "a"	*Parameter "b"*	*Reference*
Hyphema	10.6	0.0005	Duma 2005
Lens Dislocation	7.38	0.0004	Duma 2005
Retinal Damage	71.47	0.0023	Duma 2005
Globe Rupture	9.123	0.00025684	Kennedy 2006

RESULTS

A total of 73 water stream impact tests were designed to impact the eye with different nozzle sizes at a range of velocities (Figure 17). The tests resulted in normalized energy levels that varied from 57.72 J/m^2 to 6401.72 J/m^2 which corresponded to 0% risk of injury for hyphema, lens dislocation, retinal damage and globe rupture. The events were documented using high speed video (Figure 18) which provided the measurement of the water velocity which resulted in a range between 2.0 m/s and 17.4 m/s. Velocity,

intraocular pressure, and injury risk were reported for each test (Table 7, Table 8, and Table 9).

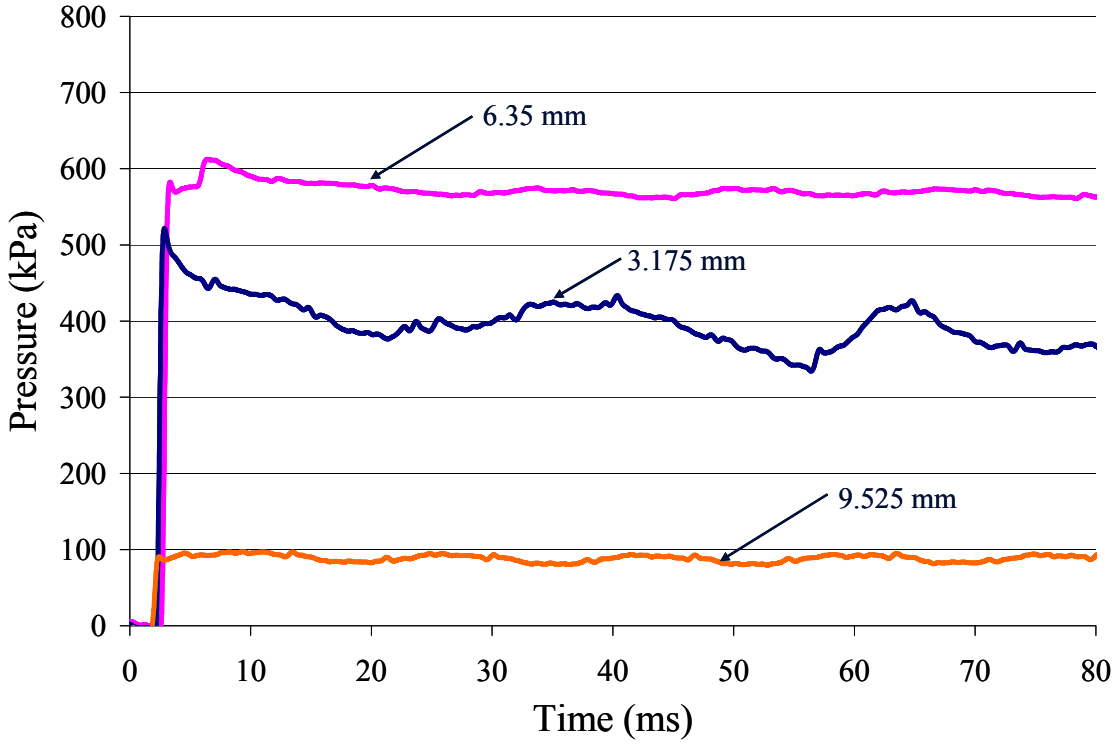

Figure 17: Intraocular pressure response for the three nozzle sizes at a water velocity of 3 m/s.

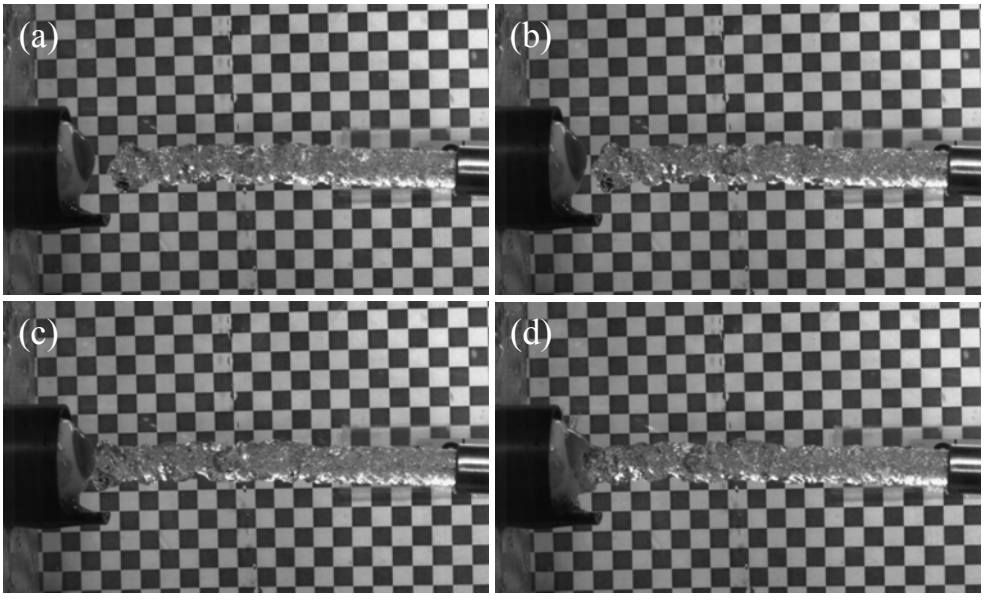

Figure 18: High speed video of a test with a 9.525 mm water stream at 4.23 m/s.

Table 7: Internal eye pressure, velocity and injury risk results for the 3.175 mm nozzle diameter water stream.

Test Number	Velocity (m/s)	Peak Internal Eye Pressure (kPa)	Injury Risk of Hyphema	Injury Risk of Lens Dislocation	Injury Risk of Retinal Damage	Injury Risk of Globe Rupture
1	3.0	723	0.00%	0.40%	0.00%	0.00%
2	4.0	714	0.00%	0.40%	0.00%	0.00%
3	5.3	673	0.00%	0.30%	0.00%	0.00%
4	6.3	673	0.00%	0.30%	0.00%	0.00%
5	11.4	693	0.00%	0.30%	0.00%	0.00%
6	4.1	459	0.00%	0.20%	0.00%	0.00%
7	5.5	473	0.00%	0.20%	0.00%	0.00%
8	6.3	478	0.00%	0.20%	0.00%	0.00%
9	7.0	549	0.00%	0.20%	0.00%	0.00%
10	3.4	522	0.00%	0.20%	0.00%	0.00%
11	11.1	470	0.00%	0.20%	0.00%	0.00%
12	5.9	437	0.00%	0.20%	0.00%	0.00%
13	6.5	452	0.00%	0.20%	0.00%	0.00%
14	8.1	439	0.00%	0.20%	0.00%	0.00%
15	2.9	507	0.00%	0.20%	0.00%	0.00%
16	3.7	509	0.00%	0.20%	0.00%	0.00%
17	10.5	512	0.00%	0.20%	0.00%	0.00%
18	17.4	421	0.00%	0.10%	0.00%	0.00%
19	8.3	434	0.00%	0.10%	0.00%	0.00%
20	6.1	463	0.00%	0.20%	0.00%	0.00%
21	3.2	474	0.00%	0.20%	0.00%	0.00%
22	4.0	433	0.00%	0.10%	0.00%	0.00%
23	5.4	418	0.00%	0.10%	0.00%	0.00%
24	10.3	453	0.00%	0.20%	0.00%	0.00%

Table 8: Internal eye pressure, velocity and injury risk results for the 6.35 mm nozzle diameter water stream.

Test Number	Velocity (m/s)	Peak Internal Eye Pressure (kPa)	Injury Risk of Hyphema	Injury Risk of Lens Dislocation	Injury Risk of Retinal Damage	Injury Risk of Globe Rupture
1	6.6	407	0.00%	0.10%	0.00%	0.00%
2	4.0	432	0.00%	0.10%	0.00%	0.00%
3	3.1	414	0.00%	0.10%	0.00%	0.00%
4	4.3	423	0.00%	0.10%	0.00%	0.00%
5	3.5	566	0.00%	0.20%	0.00%	0.00%
6	3.6	612	0.00%	0.30%	0.00%	0.00%
7	4.5	651	0.00%	0.30%	0.00%	0.00%
8	5.3	669	0.00%	0.30%	0.00%	0.00%
9	5.9	618	0.00%	0.30%	0.00%	0.00%
10	4.7	607	0.00%	0.30%	0.00%	0.00%
11	5.6	614	0.00%	0.30%	0.00%	0.00%
12	6.5	604	0.00%	0.30%	0.00%	0.00%
13	3.3	545	0.00%	0.20%	0.00%	0.00%
14	3.9	547	0.00%	0.20%	0.00%	0.00%
15	5.5	760	0.00%	0.40%	0.00%	0.00%
16	7.6	807	0.00%	0.50%	0.00%	0.00%
17	3.1	909	0.10%	0.80%	0.00%	0.10%
18	3.9	818	0.00%	0.50%	0.00%	0.00%
19	4.9	754	0.00%	0.40%	0.00%	0.00%

Table 9: Internal eye pressure, velocity and injury risk results for the 9.525mm nozzle diameter water stream.

Test Number	Velocity (m/s)	Peak Internal Eye Pressure (kPa)	Injury Risk of Hyphema	Injury Risk of Lens Dislocation	Injury Risk of Retinal Damage	Injury Risk of Globe Rupture
1	2.1	91	0.00%	0.10%	0.00%	0.00%
2	2.0	129	0.00%	0.10%	0.00%	0.00%
3	2.7	131	0.00%	0.10%	0.00%	0.00%
4	4.2	92	0.00%	0.10%	0.00%	0.00%
5	3.8	41	0.00%	0.10%	0.00%	0.00%
6	4.5	26	0.00%	0.10%	0.00%	0.00%
7	3.1	22	0.00%	0.10%	0.00%	0.00%
8	3.8	32	0.00%	0.10%	0.00%	0.00%
9	4.2	31	0.00%	0.10%	0.00%	0.00%
10	4.7	33	0.00%	0.10%	0.00%	0.00%
11	5.7	38	0.00%	0.10%	0.00%	0.00%
12	2.7	28	0.00%	0.10%	0.00%	0.00%
13	4.5	50	0.00%	0.10%	0.00%	0.00%
14	4.8	51	0.00%	0.10%	0.00%	0.00%
15	5.8	50	0.00%	0.10%	0.00%	0.00%
16	6.1	47	0.00%	0.10%	0.00%	0.00%
17	3.9	50	0.00%	0.10%	0.00%	0.00%
18	2.7	46	0.00%	0.10%	0.00%	0.00%
19	2.2	115	0.00%	0.10%	0.00%	0.00%
20	3.2	97	0.00%	0.10%	0.00%	0.00%
21	3.5	97	0.00%	0.10%	0.00%	0.00%
22	4.2	81	0.00%	0.10%	0.00%	0.00%
23	4.7	76	0.00%	0.10%	0.00%	0.00%
24	2.4	85	0.00%	0.10%	0.00%	0.00%
25	3.6	84	0.00%	0.10%	0.00%	0.00%
26	4.5	82	0.00%	0.10%	0.00%	0.00%
27	5.0	90	0.00%	0.10%	0.00%	0.00%
28	4.9	90	0.00%	0.10%	0.00%	0.00%
29	5.0	91	0.00%	0.10%	0.00%	0.00%
30	5.1	97	0.00%	0.10%	0.00%	0.00%

COMMENT

Influence of nozzle diameter and velocity were difficult to detect due to the small ranges observed for both factors (Figure 19). Although there was a slight increase in pressure as the velocity increased, there was not a strong correlation. In terms of nozzle diameter, it was found that the largest nozzle diameter had lower pressure for all velocities compared to the two smaller diameters. To fully understand the relationship between velocity,

nozzle diameter and pressure within the eye, more data should be collected for a larger range of velocities.

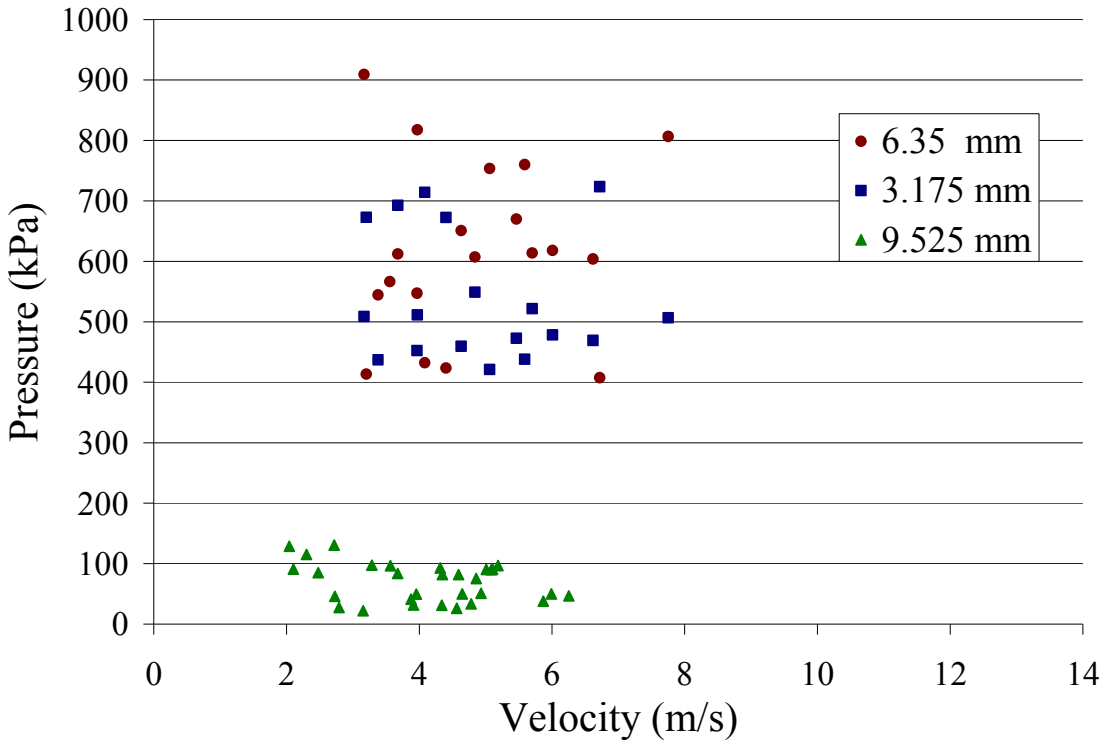

Figure 19: Influence of nozzle diameter and velocity based on intraocular pressure.

Duma et al also reported injury risk functions for corneal abrasion[17]. The current study chose not to report results for corneal abrasion due the difference in injury mechanism. It was realistic to consider that a water stream impact could cause hyphema, lens dislocation, retinal damage and globe rupture but due to the deformable nature of a water impact corneal abrasion is unlikely. The lack of case studies showing these injuries supports this finding. Because corneal abrasion is caused by the scraping away of the corneal surface, an impact with a water stream is unlikely to cause this injury. Although, it is feasible that the water stream could deposit debris into the eye which would cause corneal abrasion that was not the purpose of the current investigation.

In support of the results showing 0% risk of injury for the experimental water impacts, there is a lack of injuries in medical reports. The available case studies for water impacts involve industrial pumps, agricultural irrigation equipment, and fire hoses at high water

velocities. One of the case studies involved an agricultural irrigation line with a water velocity of 28.96 m/s[19]. In this case, a farmer was struck with the water stream and received multiple lacerations and a severed artery in the eye. A rare and severe case involved an industrial pump line with water traveling at 182.9 m/s[20]. A man was tightening a leaking pipe when it burst and hit him directly in the eye. His extra ocular muscles were torn from the globe insertions and his eye was enucleated. These cases are rare and occur with high water velocities in the range of 25 m/s to 200 m/s. In an effort to continue to understand the response of the human eye to dynamic impacts, future work should investigate higher velocity water impacts. This will help to determine thresholds based on water velocity to aid in the design of interactive water displays and water toys.

ACKNOWLEDGEMENTS

The authors would like to acknowledge the Virginia Tech - Wake Forest Center for Injury Biomechanics for funding this research.

REFERENCES

1. Frick KD, Gower EW, Kempen JH, Wolff JL. Economic impact of visual impairment and blindness in the United States. *Arch Ophthalmol.* Apr 2007;125(4):544-550.

2. Rein DB, Zhang P, Wirth KE, et al. The economic burden of major adult visual disorders in the United States. *Arch Ophthalmol.* Dec 2006;124(12):1754-1760.

3. Kennedy EA, Ng TP, McNally C, Stitzel JD, Duma SM. Risk functions for human and porcine eye rupture based on projectile characteristics of blunt objects. *Stapp Car Crash Journal.* 2006;50:651-671.

4. Vinger PF, Duma SM, Crandall J. Baseball hardness as a risk factor for eye injuries. *Arch Ophthalmol.* Mar 1999;117(3):354-358.

5. Duma SM, Jernigan MV, Stitzel JD, et al. The effect of frontal air bags on eye injury patterns in automobile crashes. *Arch Ophthalmol.* Nov 2002;120(11):1517-1522.

6. Fukagawa K, Tsubota K, Kimura C, et al. Corneal endothelial cell loss induced by air bags. *Ophthalmology.* 1993;100(12).

7. Kennedy EA, Voorhies KD, Herring IP, Rath AL, Duma SM. Prediction of severe eye injuries in automobile accidents: static and dynamic rupture pressure of the eye. *Association for the Advancement of Automotive Medicine.* 2004;48:165-179.

8. Kisielewicz LT, Kodama N, Ohno S, Uchio E. Numerical prediction of airbag caused injuries on eyeballs after radial keratotomy. Paper presented at: SAE International Congress and Exposition, 1998; Detroit, Michigan.
9. Duma SM, Crandall JR. Eye injuries from airbags with seamless module covers. *The Journal of Trauma.* 2000;48(4):786-789.
10. Duma SM, Kress TA, Porta DJ, et al. Airbag-induced eye injuries: A report of 25 cases. *The Journal of Trauma.* 1996;41(1):114-119.
11. Heier JS, Enzenauer RW, Wintermeyer SF. Ocular injuries and diseases at a combat support hospital in support of Operations Desert Shield and Desert Storm. *Archives of Ophthalmology.* 1993;111:795-798.
12. McGwin G, Xie A, Owsley C. Rate of eye injury in the United States. *Arch Ophthalmol.* 2005;123:970-976.
13. More than half a million americans suffer eye injuries from sports-related accidents: Lack of proper eye protection can lead to painful injuries, vision loss and even blindness, Vision News, (2007).
14. United States Eye Injury Registry. *Eye trauma: Epidemiology and prevention* [http://www.useironline.org/Prevention.htm. Accessed March 11, 2009.
15. Deng Z, Guensch GR, McKinstry CA, Mueller RP, Dauble DD, Richmond MC. Evaluation of fish-injury mechanisms during exposure to turbulent shear flow. *Can. J. Fish. Sci. Aquat.* 2005;62:1513-1522.
16. Nietzel DA, Richmond MC, Dauble DD, et al. *Laboratory studies on the effects of shear on fish*: United States Department of Energy; 2000.
17. Duma SM, Ng TP, Kennedy EA, Stitzel JD, Herring IP, Kuhn F. Determination of significant parameters for eye injury risk from projectiles. *Journal of Trauma.* 2005(59):960-964.
18. Bisplinghoff JA, McNally C, Duma SM. High rate internal pressurization of human eye to predict globe rupture. *Arch Ophthalmol.* April 2009.
19. *Ranch worker killed by pressurized water striking eye*: Fatality assessment and control evaluation program; 2006. 06-OR-025.
20. DeAngelis DD, Oestreicher JH. Traumatic enucleation from a high-pressure water jet. *Arch Ophthalmol.* Jan 1999;117(1):127-128.

CHAPTER 5: EVALUATION OF EYE INJURY RISK FROM PROJECTILE SHOOTING TOYS USING THE FOCUS HEADFORM

ABSTRACT

Half of eye injuries in the United States are caused by a blunt impact and more specifically, eye injuries effecting children often result from projectile shooting toys. The purpose of this study is to evaluate the risk of eye injuries of currently available projectile shooting toys. In order to assess the risk of each toy, a Facial and Ocular Countermeasure Safety (FOCUS) headform was used to measure the force applied to the eye during each hit for a total of 18 tests. The selected toys included a dart gun, a foam launcher, and a ball launcher. The force ranged from 4-93 N and was analyzed using the injury risk function for globe rupture for the FOCUS headform. Projectile characteristics were also examined using normalized energy to determine risk of corneal abrasion, hyphema, lens dislocation, retinal damage and globe rupture. It was found that the three toys tested produced peak loads corresponding with risk of globe rupture between 0% and 17.3%. The normalized energy results show no risk of hyphema, lens dislocation, retinal damage or globe rupture and a maximum risk of corneal abrasion of 5.9%. This study concludes that although there are many eye injuries caused by projectiles, the selected toys show a very low risk of eye injury.

Keywords: FOCUS, headform, eye, injury, projectile, toy, gun

INTRODUCTION

According to a 2002 study, an estimated 165,200 children were treated in emergency rooms for toy related injuries [1]. Over 1.9 million people suffer from eye injuries in the United States each year [2]. Within the civilian population, nearly half of these injuries are caused by a blunt impact and more specifically, eye injuries effecting children often result from toys that shoot plastic projectiles [3]. High speed projectiles are the cause of some of the most severe eye injuries. Paintballs, fireworks, Airsoft guns and BB guns are

all responsible for a large number of ocular injuries each year due to their ability to produce high velocities and the availability of these products [4-6]. While some studies have looked at the risk of eye injury from Airsoft pellet impacts, projectile impacts, and automobile crash scenarios, there are no current studies that have quantified injury risk for projectile shooting toys [7-11]. Therefore the purpose of this study is to evaluate the risk of eye injury of currently available projectile shooting toys.

METHODOLOGY

In order to evaluate the risk of eye injury for each toy, an advanced Facial and Ocular Countermeasure Safety (FOCUS) headform was used to measure the force applied to the synthetic eye during each hit. The FOCUS was designed and validated to evaluate potential globe rupture injuries, as well as, aid in safety equipment design and overall injury protection [12]. Force deflection response for human eyes *ex-vivo* and *in-situ* were determined and compared to the force deflection response of the synthetic eye and synthetic orbit assembly to ensure a biofidelic response. Experimental tests were conducted to develop an injury risk curve for the FOCUS headform based on the eye load cell [12, 13]. Assessment of three toys included a foam dart gun, foam launcher, and a ball launcher. Each toy was positioned in front of the FOCUS and aligned to hit the right eye (Figure 20). Force data from the right eye load cell were collected using a data acquisition system at 20,000 Hz and projectile velocity was measured using high speed video taken at 2100 frames/sec with a resolution of 512x256. Force data were filtered using CFC 1000 according to SAE J211/1 [14].

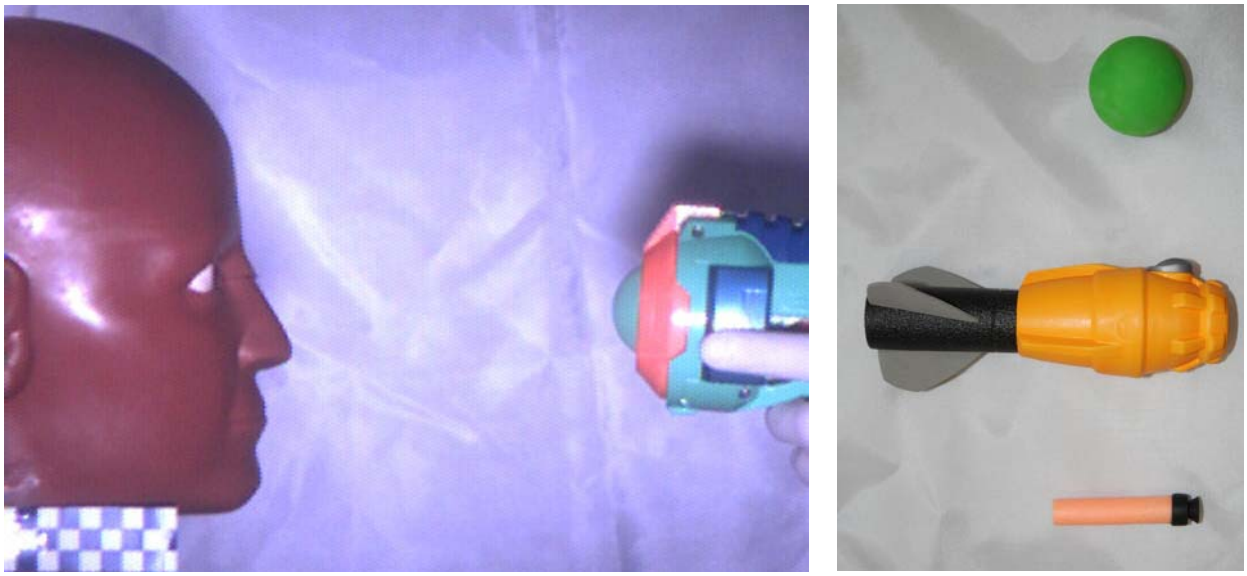

Figure 20: (Left) Experimental setup with the FOCUS headform and the ball launcher. (Right) Relative size comparison of the three projectiles. Top to bottom: ball, foam launcher, dart.

In the previous FOCUS validation study, projectile tests were conducted to develop a conservative injury risk criteria based on the response of the eye load cell [12]. The injury risk curve generated was used in the current study to evaluate the risk of globe rupture for each toy impact (Equation 1). Force traces were analyzed and the peak load was found for each test. The probability of globe rupture was then calculated based on the injury risk criteria reported by Kennedy et al [12].

$$\text{ProbabilityofInjury}(\%) = \frac{1}{1 + e^{11.94 - (0.1119)(\text{PeakLoad})}} \qquad \text{(eq.1)}$$

In order to evaluate additional eye injuries such as corneal abrasion, hyphema, lens dislocation, retinal damage, and globe rupture, normalized energy was used to determine the risk of injury. Previous research concluded that normalized energy was the most significant predictor of eye injury above kinetic energy [10]. Normalized energy was defined as the kinetic energy divided by the cross-sectional area of the object. This calculation included the mass (m), velocity (v) and cross-sectional area of the object (A) (Equation 2).

$$\text{Normalized Energy} = \frac{\text{Kinetic Energy}}{\text{Projected Area}} = \frac{\frac{1}{2}\text{mv}^2}{\text{A}} \qquad \text{(eq.2)}$$

Injury risk curves using normalized energy as the injury predictor have been previously developed for corneal abrasion, hyphema, lens dislocation, retinal damage, and globe rupture [10, 13] which were utilized in the current study (Figure 21). Normalized energy and risk of injury for each eye injury (corneal abrasion, hyphema, lens dislocation, retinal damage, and globe rupture) were determined using the injury risk function coefficients determined from published research [10, 13] (Table 10). Similar to the injury risk function developed for the FOCUS eye load cell, a general form of the injury risk function (Equation 3) was used to express a relationship between normalized energy (x) and the probability of injury. Parameters "a" and "b" refer to constants that have been determined by the previous studies through logistic regression and are unique to the specific predictor. Risk of injury for corneal abrasion, hyphema, lens dislocation, retinal damage, and globe rupture were calculated using the normalized energy method for a total of 18 tests.

$$\text{Probability of Injury}(\%) = \frac{1}{1+e^{a-bx}} \qquad \text{(eq.3)}$$

Table 10: Injury risk function coefficients from published research.

	Parameter "a"	*Parameter "b"*	*Reference*
Corneal Abrasion	5.03	0.0034	Duma 2005
Hyphema	10.6	0.0005	Duma 2005
Lens Dislocation	7.38	0.0004	Duma 2005
Retinal Damage	71.47	0.0023	Duma 2005
Globe Rupture	9.123	0.00025684	Kennedy 2006

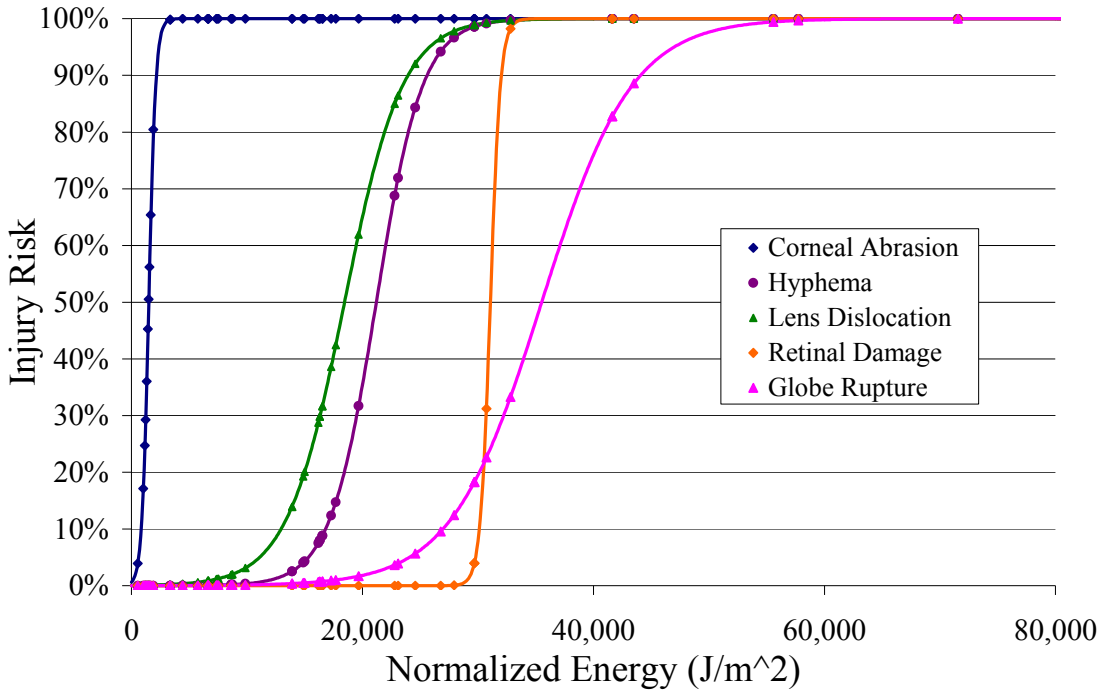

Figure 21: Injury risk curves for corneal abrasion, hyphema, lens dislocation, retinal damage, and globe rupture as a function of normalized energy from published research.

RESULTS

The analysis of injury risk developed using the FOCUS eye load cell force produced risk of globe rupture between 0% and 17.3% (Table 11). Injury risk results from the normalized energy technique for corneal abrasion, hyphema, lens dislocation, retinal damage and globe rupture ranged from 0% to 5.9% (Table 12). Although risk of globe rupture from the load analysis showed injury risk of 17.3%, the analysis from normalized energy for that test showed 0% risk of injury for hyphema, lens dislocation, retinal damage, and globe rupture. The highest risk of injury reported for all 18 tests from the projectile characteristics was 5.9% risk of corneal abrasion.

The foam launcher produced the largest risk of globe rupture based on FOCUS eye load cell force yet reported 0% risk of globe rupture based on projectile characteristics, and only 1.9% - 3.9% risk of corneal abrasion. In contrast, the injury risk for globe rupture as a function of force for the dart gun was 0.0%, yet produced the largest risk of corneal

abrasion calculated from normalized energy. Risk of injury for the ball launcher calculated from both force and normalized energy resulted in low injury risk values. The maximum value for that toy was 0.3% risk of globe rupture.

Table 11: Globe rupture injury risk results from FOCUS eye load cell injury risk criteria.

Test #	Toy	Mass (kg)	Peak eye force (N)	Risk of Globe Rupture
1	Dart Gun	0.001686	26.17	0.00%
2	Dart Gun	0.001686	12.79	0.00%
3	Dart Gun	0.001686	15.5	0.00%
4	Dart Gun	0.001686	13.85	0.00%
5	Dart Gun	0.001686	7.66	0.00%
6	Dart Gun	0.001686	17.61	0.00%
7	Dart Gun	0.001686	11.87	0.00%
8	Dart Gun	0.001686	15.43	0.00%
9	Dart Gun	0.001686	7.48	0.00%
10	Foam Launcher	0.007409	92.74	17.30%
11	Foam Launcher	0.007409	60.24	0.50%
12	Foam Launcher	0.007409	44.83	0.10%
13	Foam Launcher	0.007409	84.24	7.50%
14	Foam Launcher	0.007409	83.28	6.80%
15	Ball Launcher	0.004965	54.43	0.30%
16	Ball Launcher	0.004965	26.59	0.00%
17	Ball Launcher	0.004965	4.21	0.00%
18	Ball Launcher	0.004965	42.71	0.10%

Table 12: Injury risk results using the normalized energy method for corneal abrasion, hyphema, lens dislocation, retinal damage, and globe rupture.

Test #	Toy	Normalized Energy (J/m^2)	Risk of Corneal Abrasion	Risk of Hyphema	Risk of Lens Dislocation	Risk of Retinal Damage	Risk of Globe Rupture
1	Dart Gun	662.35	5.9%	0.0%	0.1%	0.0%	0.0%
2	Dart Gun	613.30	5.0%	0.0%	0.1%	0.0%	0.0%
3	Dart Gun	613.30	5.0%	0.0%	0.1%	0.0%	0.0%
4	Dart Gun	659.23	5.8%	0.0%	0.1%	0.0%	0.0%
5	Dart Gun	623.65	5.2%	0.0%	0.1%	0.0%	0.0%
6	Dart Gun	566.14	4.3%	0.0%	0.1%	0.0%	0.0%
7	Dart Gun	592.86	4.7%	0.0%	0.1%	0.0%	0.0%
8	Dart Gun	592.86	4.7%	0.0%	0.1%	0.0%	0.0%
9	Dart Gun	631.47	5.3%	0.0%	0.1%	0.0%	0.0%
10	Foam Launcher	490.30	3.3%	0.0%	0.1%	0.0%	0.0%
11	Foam Launcher	323.67	1.9%	0.0%	0.1%	0.0%	0.0%
12	Foam Launcher	521.42	3.7%	0.0%	0.1%	0.0%	0.0%
13	Foam Launcher	537.34	3.9%	0.0%	0.1%	0.0%	0.0%
14	Foam Launcher	430.92	2.8%	0.0%	0.1%	0.0%	0.0%
15	Ball Launcher	180.58	1.2%	0.0%	0.1%	0.0%	0.0%
16	Ball Launcher	180.58	1.2%	0.0%	0.1%	0.0%	0.0%
17	Ball Launcher	177.79	1.2%	0.0%	0.1%	0.0%	0.0%
18	Ball Launcher	156.26	1.1%	0.0%	0.1%	0.0%	0.0%

DISCUSSION

The purpose of this study was to evaluate the risk of eye injuries for three currently available projectile shooting toys: a dart gun, foam launcher, and ball launcher. Two methodologies were used in order to evaluate the injury risk. Results produced from the analysis using the FOCUS eye load cell force showed that three of the foam launcher tests (test #10, 13, 14) produced risk of globe rupture. The same tests using the normalized energy method resulted in 0% risk of hyphema, lens dislocation, retinal damage, and globe rupture, while producing only 3.4%, 3.9% and 2.8% risk of corneal

abrasion. Although the foam launcher produced peak forces that were predicted to cause globe rupture, the contact area of the projectile was large enough to produce a normalized energy that predicted no injury. A limitation of the FOCUS globe rupture injury risk function is projectile specificity. Impact tests were performed with only BBs to determine the risk function and therefore it is a conservative estimate for larger projectiles [13]. Determination of injury risk should be based on projectile characteristics when possible, as was done in the current study.

Eye injury risk values calculated as a function of normalized energy showed positive results for the safety of the tested toys. Additionally, the presented injury risk values were conservative because they were based on the projectile characteristics and were assumed to have a direct hit to the eye. Because every hit to the eye was not a direct hit, the normalized energy method produced an overestimation of the injury risk.

CONCLUSION

This study used the FOCUS headform and projectile characteristics to evaluate risk of eye injury of three currently available projectile shooting toys. Risk of globe rupture was calculated using a previously developed injury risk curve and the measured force from the FOCUS eye load cell. The force ranged from 4-93 N which resulted in 0-17.3% risk of globe rupture. Due to the projectile specificity of the FOCUS load cell injury criteria, a normalized energy approach should be utilized when possible. Therefore, projectile characteristics were used to calculate normalized energy to determine risk of injury for corneal abrasion, hyphema, lens dislocation, retinal damage, and globe rupture. Results showed 0% risk of hyphema, lens dislocation, retinal damage, and globe rupture, and a low risk of corneal abrasion (0-6%). This study concludes that the selected projectile shooting toys show a very low risk of injury.

ACKNOWLEDGEMENTS

The authors would like to acknowledge the Virginia Tech-Wake Forest Center for Injury Biomechanics for supporting this research.

REFERENCES

[1] M. Stephenson, "Danger in the toy box," *Journal of Pediatric Health Care,* vol. 19, pp. 187-189, 2005.

[2] G. McGwin, A. Xie, and C. Owsley, "Rate of eye injury in the united states," *Archives of Ophthalmology,* vol. 123, pp. 970-976, 2005.

[3] "American Academy of Pediatrics Committee on Accident and Poison Prevention: Injuries related to "toy" firearms," *Pediatrics,* vol. 79, pp. 473-4, Mar 1987.

[4] F. Kuhn, R. Morris, D. C. Witherspoon, L. Mann, V. Mester, L. Modis, and A. Berta, "Serious firworks-related eye injuries," *Ophthalmic Epidemiology,* vol. 7, pp. 139-148, 2000.

[5] P. F. Vinger, J. J. Sparks, K. R. Mussack, J. Dondero, and J. B. Jeffers, "A program to prevent eye injuries in paintball," *Sports Vision,* vol. 33, pp. 33-40, 1997.

[6] J. C. Fleischhauer, D. Goldblum, B. E. Frueh, and F. Koerner, "Ocular injuries cause by airsoft guns," *Arch Ophthalmol,* vol. 117, pp. 1437-1439, 1999.

[7] S. M. Duma and J. R. Crandall, "Eye injuries from airbags with seamless module covers," *The Journal of Trauma,* vol. 48, pp. 786-789, 2000.

[8] S. M. Duma, M. V. Jernigan, J. D. Stitzel, I. P. Herring, J. S. Crowley, F. T. Brozoski, and C. R. Bass, "The effect of frontal air bags on eye injury patterns in automobile crashes," *Arch Ophthalmol,* vol. 120, pp. 1517-22, Nov 2002.

[9] S. M. Duma, T. A. Kress, D. J. Porta, C. D. Woods, J. N. Snider, P. M. Fuller, and R. J. Simmons, "Airbag-induced eye injuries: A report of 25 cases," *The Journal of Trauma,* vol. 41, pp. 114-119, 1996.

[10] S. M. Duma, T. P. Ng, E. A. Kennedy, J. D. Stitzel, I. P. Herring, and F. Kuhn, "Determination of significant parameters for eye injury risk from projectiles," *Journal of Trauma,* pp. 960-964, 2005.

[11] E. A. Kennedy, T. P. Ng, and S. M. Duma, "Evaluating eye injury risk of Airsoft pellet guns by parametric risk functions," *Biomed Sci Instrum,* vol. 42, pp. 7-12, 2006.

[12] E. A. Kennedy, J. A. Inzana, C. McNally, S. M. Duma, P. J. Depinet, K. H. Sullenberger, C. R. Morgan, and F. T. Brozoski, "Development and validation of a synthetic eye and orbit for estimating the potential for globe rupture due to specific impact conditions," *Stapp Car Crash Journal,* vol. 51, pp. 381-400, October 2007 2007.

[13] E. A. Kennedy, T. P. Ng, C. McNally, J. D. Stitzel, and S. M. Duma, "Risk functions for human and porcine eye rupture based on projectile characteristics of blunt objects," *Stapp Car Crash Journal,* vol. 50, pp. 651-671, 2006.

[14] SAE. "Instrumentation for impact test - part 1: electronic instrumentation " SAE paper no. J211/1. Warrendale, PA, S. o. A. Engineers, 1995.

CHAPTER 6: SUMMARY OF RESEARCH

The research presented in this thesis will be published in scientific journals and presented at relevant conferences. Chapters one through five have been formatted to represent the journal or conference in which it will be submitted. The titles and corresponding journals and/or conferences for each chapter are listed in Table 13.

Table 13: List of publications as an outcome of this thesis.

Chapter	**Title**	**Journal / (*Conference*)**
1	High Rate Internal Pressurization of Human Eyes to Predict Globe Rupture	Archives of Ophthalmology* *(Biomedical Sciences Instrumentation)**
2	Dynamic Material Properties of the Human Sclera	Journal of Biomechanics* *(Biomedical Sciences Instrumentation)**
3	Intraocular Pressure During High Speed Projectile Impacts	Archives of Ophthalmology
4	Eye Injury Risk from Water Stream Impact	Journal of Trauma
5	Evaluation of Eye Injury Risk from Projectile Shooting Toys using the FOCUS Headform	*(Biomedical Sciences Instrumentation)**

* Accepted